KIAS-P15035

Three loop neutrino model with isolated $k^{\pm\pm}$

Kenji Nishiwaki,[1,*] Hiroshi Okada,[1,2,†] and Yuta Orikasa[1,3,‡]

[1]*School of Physics, Korea Institute for Advanced Study, Seoul 130-722, Republic of Korea*

[2]*Physics Division, National Center for Theoretical Sciences, National Tsing-Hua University, Hsinchu 30013, Taiwan*

[3]*Department of Physics and Astronomy, Seoul National University, Seoul 151-742, Republic of Korea*

(Dated: October 26, 2018)

arXiv:1507.02412v3 [hep-ph] 27 Nov 2015

Abstract

We propose a three loop radiative neutrino mass scenario with an *isolated* doubly charged singlet scalar $k^{\pm\pm}$ without couplings to the charged leptons, while two other singly charged scalars $h_1^\pm$ and $h_2^\pm$ attach to them. In this setup, the lepton flavor violation originating from $k^{\pm\pm}$ exchanges is suppressed and the model is less constrained, where some couplings can take sizable values. As reported in our previous work [1], the loop suppression factor at the three loop level would be too strong and realized neutrino masses in a three loop scenario could be smaller than the observed minuscule values. The sizable couplings can help us to *enhance* neutrino masses without drastically large scalar trilinear couplings appearing in a neutrino mass matrix, which tends to drive the vacuum stability to become jeopardized at the one loop level. Now the doubly charged scalar $k^{\pm\pm}$ has less constraint via lepton flavor violation and the vacuum can be quite stable, and thus a few hundred GeV mass in $k^{\pm\pm}$ is possible, which is within the LHC reach and this model can be tested in the near future. Note that the other $h_1^\pm$ and $h_2^\pm$ should be heavy at least around a few TeV. We suitably arrange the charges of an additional global $U(1)$ symmetry, where the decay constant of the associated Nambu-Goldstone boson can be around a TeV scale consistently. Also, this model is indirectly limited through a global analysis on results of the LHC Higgs search and issues on a dark matter candidate, the lightest Majorana neutrino. After $h_1^\pm$ and $h_2^\pm$ are decoupled, this particle couples to the standard model particles only through two charge parity even scalars in theory and thus information on this scalar sector is important. Consistent solutions are found, but a part of them is now on the edge.

Keywords: Neutrinos, Dark Matter

*Electronic address: nishiken@kias.re.kr

†Electronic address: macokada3hiroshi@gmail.com

‡Electronic address: orikasa@kias.re.kr

I. INTRODUCTION

Recently, the second round of the physics run at the Large Hadron Collider (LHC) started and a magnificent operation for exploring the scalar sector describing the electroweak (EW) scale was launched. The greatest achievement at the first run of the LHC is the observation of the new Higgs-like scalar boson, which was the last missing piece of the standard model (SM), around 125 GeV by the ATLAS and the CMS experiments [2, 3].

The Yukawa couplings to heavy fermions of the SM, namely the top and bottom quarks and the tau lepton have been surveyed with good precision, whereas the lighter states are still mysterious from both the experimental and theoretical point of view. The extremely tiny observed masses of active components of the neutrinos would be key to investigating the scalar sector theoretically because we should accept at least 10^{12}-order hierarchy in the Higgs Yukawa couplings for describing the neutrino nature within the SM.

One of the most stimulating ideas for addressing this issue is radiative generations of the neutrino profiles. Loop suppression factors should appear in the neutrino masses in this type of scenario, which help to alleviate the hierarchy in couplings. Another motivation for this direction is that the continuous and/or discrete symmetries ensuring the loop origin could also guarantee the existence of a (or multiple) dark matter (DM) candidate(s). Following the landmarks [4–8], recently a variety of works on radiative seesaw model have been done [9]–[59], where we can also find studies emphasizing non-Abelian discrete symmetry [60–67], radiative generation of quark/charged lepton masses [68–72], operator analysis [73, 74], radiative models accompanying conformal EW symmetry breaking [75–77], and others [78–90].

From the naturalness point of view, higher-loop generation is better. The first three loop model for a natural explanation of the neutrino profiles was proposed in Ref. [7] and the following works continue [1, 13, 35, 43–45, 47, 51, 52, 56, 57, 62, 88], where in such situations, couplings related with the neutrino masses can be close to unity compared with those in models with one or two loop level generation.

On the other hand, three loop generations could face problems owing to the largeness of couplings. As discussed in Ref. [1], the three loop suppression factor $1/(4\pi)^6$ sometimes looks very strong and we probably *enhance* part of couplings for a suitable realization of the neutrino masses. Considering large Yukawa-type couplings with lepton flavor viola-

tion (LFV) tend to result in unacceptable enhancements in LFV processes. Hence, choosing sizable scalar trilinear couplings appearing in the neutrino mass matrix, which do not generate LFV directory, seems to be a reasonable prescription. But this diagnosis could still be at least partly a misjudgment. When we go for one loop level, as shown in Ref. [1], these substantial trilinear couplings give drastic negative contributions to quartic couplings of charged scalar bosons and the vacuum can be threatened with being destabilized. The last option would be to accept decouplings of additional charged bosons, namely around 10 TeV, where the neutrino profile itself can be suitably generated. But finding clear signals at colliders becomes very difficult even at the updated 13 or 14 TeV LHC.

To circumvent the situation, we propose a refined three loop model by use of a global $U(1)$ symmetry without additional discrete symmetry. A key point is introducing additional Majorana neutrinos, which can violate lepton flavors in the fermion line inside diagrams describing the neutrino masses. It is important that with the above setup, a doubly charged scalar $k^{\pm\pm}$ no longer needs to have direct couplings to the charged leptons. We mention that in our previous model without Majorana neutrinos in Ref. [1], like in the Zee-Babu model [6], a doubly charged scalar should attach the charged leptons to generate violation in lepton flavors, where tree-level lepton flavor violating processes are generated and we cannot put large values in the corresponding couplings consistently.

In the present $k^{\pm\pm}$-*isolated* scenario, the doubly charged scalar $k^{\pm\pm}$ is quarantined from the charged lepton sector at the leading order by a suitable choice of global $U(1)$ charges. Now, $k^{\pm\pm}$ cannot contribute to phenomena with LFV at the leading order and constraints on couplings are weakened. Consequently, the scalar trilinear couplings can take smaller values and the vacuum stability would not be so serious even when we consider a few hundred GeV $k^{\pm\pm}$, the detection of which can be an evident signal for probing this scenario at the LHC experiments.

This paper is organized as follows. In Sec. II, first we introduce our setups and subsequently, we discuss miscellaneous issues in this model, namely, forms of scalar masses and mixings, properties of the Nambu-Goldstone (NG) boson associated with the breakdown of the global $U(1)$ symmetry, sizable correction via charged scalars to vacuum stability, form of the active neutrino mass matrix at the three loop level, and details on processes accompanying LFV in order. In the following Sec. III, after having a discussion on analogies with the Zee-Babu model [6], we execute parameter scans both in the normal and inverted hier-

archies. In Sec. IV, we make global fits of signal strengths of the Higgs production in various channels announced by the ATLAS and the CMS experiments, which restrict possible values of the mass of the doubly charged scalar and the mixing angle between the SM Higgs boson and an additional charge parity (CP) even scalars, whose vacuum expectation value (VEV) breaks the global $U(1)$ symmetry. In Sec. V, we discuss properties of the dark matter candidate of this scenario, which is the lightest right-hand neutrino, through a relic density calculation, an estimation of the invisible decay width of the observed 125 GeV scalar and an evaluation of spin-independent direct detection cross section. Section VI is devoted to summarizing results and making conclusions. In Appendix A, we give analytic forms of the loop functions describing lepton-flavor-violating processes. In Appendix B, a part of partial decay widths of the two CP even scalars with nontrivial forms is described. In Appendix C, we summarize the averaged matrix elements squared for relic density calculation.

II. BASIC ISSUES ON THE SCENARIO

A. Model setup

We discuss a three loop induced radiative neutrino model with a $U(1)$ global symmetry. The particle contents and their charges are shown in Table I. We introduce three Majorana fermions $N_{R_{1,2,3}}$ and new bosons; one gauge-singlet neutral boson Σ_0, two singly charged singlet scalars $(h_1^\pm, h_2^\pm)$, and one gauge-singlet doubly charged boson $k^{\pm\pm}$ to the SM. We assume that only the SM-like Higgs Φ and the additional neutral scalar Σ_0 have VEVs, which are symbolized as $\langle\Phi\rangle \equiv v/\sqrt{2}$ and $\langle\Sigma_0\rangle \equiv v'/\sqrt{2}$, respectively. Here, we set v as $\simeq 246\,\mathrm{GeV}$. It is natural that v' is greater than v to some extent to evade a large mixing, which is constrained by the LHC data; see Sec. IV for details. $x\,(\neq 0)$ is an arbitrary number of the charge of the hidden $U(1)$ symmetry,[1] and under the assignments, neutrino mass matrix is generated at the three loop level. Note that a remnant Z_2 symmetry remains after the hidden $U(1)$ symmetry breaking and the particles $N_{R_{1,2,3}}$ and $h_2^\pm$ have negative parities. Then, when a Majorana neutrino is the lightest among them, the stability is accidentally ensured.

[1] Here, we assume that this $U(1)$ symmetry is global. However, one can straightforwardly move to the local one by introducing additional fermions

	Lepton Fields			Scalar Fields				
Characters	L_{L_i}	e_{R_i}	N_{R_i}	Φ	Σ_0	h_1^+	h_2^+	k^{++}
$SU(3)_C$	**1**	**1**	**1**	**1**	**1**	**1**	**1**	**1**
$SU(2)_L$	**2**	**1**	**1**	**2**	**1**	**1**	**1**	**1**
$U(1)_Y$	$-1/2$	-1	0	$1/2$	0	1	1	2
$U(1)$	0	0	$-x$	0	$2x$	0	x	$2x$

TABLE I: Contents of lepton and scalar fields and their charge assignment under $SU(3)_C \times SU(2)_L \times U(1)_Y \times U(1)$, where $U(1)$ is an additional global symmetry and $x \neq 0$. The subscripts found in the lepton fields $i\,(=1,2,3)$ indicate generations of the fields. The bold letters emphasize that these numbers correspond to representations of the Lie groups of the NonAbelian gauge interactions.

The relevant Lagrangian for Yukawa sector $\mathcal{L}_Y$ and scalar potential $\mathcal{V}$ allowed under the global symmetry is given as

$$-\mathcal{L}_Y = (y_\ell)_{ij}\bar{L}_{L_i}\Phi e_{R_j} + \frac{1}{2}(y_L)_{ij}\bar{L}^c_{L_i}L_{L_j}h_1^+ + (y_R)_{ij}\bar{N}_{R_i}e^c_{R_j}h_2^- + \frac{1}{2}(y_N)_{ij}\Sigma_0\bar{N}^c_{R_i}N_{R_j} + \text{h.c.}, \tag{II.1}$$

$$\begin{aligned}\mathcal{V} &= m_\Phi^2|\Phi|^2 + m_\Sigma^2|\Sigma_0|^2 + m_{h_1}^2|h_1^+|^2 + m_{h_2}^2|h_2^+|^2 + m_k^2|k^{++}|^2 \\ &+ \left[\lambda_{11}\Sigma_0^* h_1^- h_1^- k^{++} + \mu_{22}h_2^+h_2^+k^{--} + \text{h.c.}\right] + \lambda_\Phi|\Phi|^4 + \lambda_{\Phi\Sigma}|\Phi|^2|\Sigma_0|^2 + \lambda_{\Phi h_1}|\Phi|^2|h_1^+|^2 \\ &+ \lambda_{\Phi h_2}|\Phi|^2|h_2^+|^2 + \lambda_{\Phi k}|\Phi|^2|k^{++}|^2 + \lambda_\Sigma|\Sigma_0|^4 + \lambda_{\Sigma h_1}|\Sigma_0|^2|h_1^+|^2 + \lambda_{\Sigma h_2}|\Sigma_0|^2|h_2^+|^2 \\ &+ \lambda_{\Sigma k}|\Sigma_0|^2|k^{++}|^2 + \lambda_{h_1}|h_1^+|^4 + \lambda_{h_1h_2}|h_1^+|^2|h_2^+|^2 + \lambda_{h_1k}|h_1^+|^2|k^{++}|^2 \\ &+ \lambda_{h_2}|h_2^+|^4 + \lambda_{h_2k}|h_2|^2|k^{++}|^2 + \lambda_k|k^{++}|^4,\end{aligned} \tag{II.2}$$

where the indices i, j indicate matter generations and the superscript "c" means charge conjugation.[2] y_L, y_R and y_N are antisymmetric, general, symmetric three-by-three matrices, respectively. The first term of $\mathcal{L}_Y$ generates the charged-lepton masses following the SM manner. Majorana mass terms are derived from the fourth one after Σ_0 obtains a VEV. Note that this VEV also generates an effective trilinear coupling μ_{11} $\left(\text{in front of } h_1^- h_1^- k^{++}\right)$

[2] For $SU(2)_L$ doublets, charge conjugation is defined with the $SU(2)_L$ rotation described by a Pauli matrix as $i\sigma_2$.

from the quartic coupling λ_{11} $\left(\text{in front of } \Sigma_0^* h_1^- h_1^- k^{++}\right)$, where the coefficient is given as

$$\mu_{11} = \lambda_{11}\langle\Sigma_0^*\rangle = \lambda_{11}\frac{v'}{\sqrt{2}}, \tag{II.3}$$

where we use the parametrization of $\langle\Sigma_0\rangle$ declared in Eq. (II.5) in the next subsection. We assume the following two things: (i) λ_{11} and μ_{22} are positive real; (ii) y_N is diagonal and obeys the hierarchy $(y_N)_{11} < (y_N)_{22} < (y_N)_{33}$ among positive-real parameters, which means that a generated Majorana mass matrix for N_R is also diagonal one and the mass ordering is $M_{N_1} < M_{N_2} < M_{N_3}$. The concrete forms of the masses are

$$M_{N_1} = \frac{v'}{\sqrt{2}}(y_N)_{11}, \quad M_{N_2} = \frac{v'}{\sqrt{2}}(y_N)_{22}, \quad M_{N_3} = \frac{v'}{\sqrt{2}}(y_N)_{33}. \tag{II.4}$$

B. Mass eigenvalues and eigenstates of scalars

The neutral scalar fields are parametrized as

$$\Phi = \begin{bmatrix} w^+ \\ \frac{v+\phi+iz}{\sqrt{2}} \end{bmatrix}, \quad \Sigma_0 = \frac{v'+\sigma}{\sqrt{2}}e^{iG/v'}. \tag{II.5}$$

where $v \simeq 246\,\text{GeV}$ is the VEV of the Higgs doublet field, and $w^\pm$ and z are (would-be) NG bosons that are absorbed as the longitudinal components of the W and Z bosons, respectively. Requiring the tadpole conditions, $\partial\mathcal{V}/\partial\phi|_v = 0$ and $\partial\mathcal{V}/\partial\sigma|_{v'} = 0$, the resultant mass matrix squared of the CP even components (ϕ, σ) is given by

$$m^2(\phi,\sigma) = \begin{bmatrix} 2\lambda_\Phi v^2 & \lambda_{\Phi\Sigma}vv' \\ \lambda_{\Phi\Sigma}vv' & 2\lambda_\Sigma v'^2 \end{bmatrix} = \begin{bmatrix} \cos\alpha & \sin\alpha \\ -\sin\alpha & \cos\alpha \end{bmatrix} \begin{bmatrix} m_h^2 & 0 \\ 0 & m_H^2 \end{bmatrix} \begin{bmatrix} \cos\alpha & -\sin\alpha \\ \sin\alpha & \cos\alpha \end{bmatrix}, \tag{II.6}$$

where h is the SM-like Higgs ($m_h = 125\,\text{GeV}$) and H is an additional CP even Higgs mass eigenstate. The mixing angle α is determined as

$$\sin 2\alpha = \frac{2\lambda_{\Phi\Sigma}vv'}{m_H^2 - m_h^2}. \tag{II.7}$$

The neutral bosons ϕ and σ are rewritten in terms of the mass eigenstates h and H as

$$\phi = h\cos\alpha + H\sin\alpha, \quad \sigma = -h\sin\alpha + H\cos\alpha. \tag{II.8}$$

A NG boson G emerges due to the spontaneous symmetry breaking of the global $U(1)$ symmetry. The mass eigenvalues for the singly charged bosons $h_1^\pm$, $h_2^\pm$ and the doubly

charged boson $k^{\pm\pm}$ are given as

$$m^2_{h_1^\pm} = m^2_{h_1} + \frac{1}{2}(\lambda_{\Phi h_1} v^2 + \lambda_{\Sigma h_1} v'^2), \quad m^2_{h_2^\pm} = m^2_{h_2} + \frac{1}{2}(\lambda_{\Phi h_2} v^2 + \lambda_{\Sigma h_2} v'^2),$$
$$m^2_{k^{\pm\pm}} = m^2_k + \frac{1}{2}(\lambda_{\Phi k} v^2 + \lambda_{\Sigma k} v'^2), \tag{II.9}$$

where the three charged particles are not mixed due to the symmetries of the system and thus they themselves are mass eigenstates.

C. Issues on the Goldstone boson

Accompanying the spontaneous breakdown of a $U(1)$ global symmetry, a NG boson emerges as an almost massless state in theory, which could play significant roles in particle physics and cosmology [91]. Like the usual Majoron case [92], our NG boson G communicates with the lepton sector.

An important characteristic of G is that, as described in Table I, the lepton doublets and the charged lepton singlets do not hold nonzero charges of the global $U(1)$. This means that no anomaly-induced interaction to two photons is generated in our setup, which puts a significant constraint on the decay constant of NG bosons [93]. Thus, in the present scenario, we can choose "lower" values around a TeV scale without doing any harm.

Another route for constraining models via NG bosons is through the active-sterile component mixing as through the lepton-flavor-violating transition like $\mu^- \to e^-$ (NG) seen in Majoron seesaw scenarios, *e.g.*, discussed in Ref. [94]. Different from such a situation in our case, the active and the sterile components cannot mix with each other since this mixture is prohibited by the residual Z_2 symmetry after the global $U(1)$ breaking shown in Table I. Then the absence of this type of constraint is assured via the accidentally remaining symmetry. The neutrinoless double beta decay via W exchanges does not restrict our scenario since the sequence with W boson also requires the active-sterile mixing. Note that the three additional charged singlet scalars have no direct coupling to the quarks and are therefore ineffective.

In contrast, the NG boson G couples to the corresponding CP even component σ, which should mix with the Higgs component of the doublet Φ. This means that G can contribute to physics associated with the CP even scalars. As we see in Sec. V, the pair annihilation

process of the dark matter candidate N_{R_1} is just an example.[3]

Finally, we briefly comment on possible bounds from cosmological issues. For example, an effect on cosmic microwave background via cosmic string generated by the spontaneous breakdown of the global $U(1)$ symmetry possibly put a constraint on our scenario. The bound discussed in Ref. [96] can be interpreted as $v' < 10^{15}\,\mathrm{GeV}$, and thus this issue is harmless. On the other hand, as we discuss later in Sec. III B, at least part of scalar self couplings tends to be $\mathcal{O}(1)$ (at around the EW scale) owing to the requirements via coexistence of the observed active neutrino profiles and the null observation in lepton-flavor-violating currents. This trend would lead to blowups of the self couplings a little bit above the lower scale that we focus on in this paper. Then it might not be so fruitful to discuss issues originating from physics at a higher scale.

D. Vacuum stability against charged scalar trilinear couplings

Vacuum stability has to be especially assured in the Higgs potential against contributions from electrically charged bosons ($h_1^\pm, h_2^\pm, k^{\pm\pm}$). However, our model has some loop contributions to leading-order values of these quartic couplings via the scalar trilinear couplings μ_{11} and μ_{22}. When they are large, we should examine the vacuum stability against the effect. Here, we examine this issue at the one loop level. Let us describe these quartic couplings as follows,

$$0 < \lambda_{h_1} = \lambda_{h_1}^{(0)} + \lambda_{h_1}^{(1)}, \tag{II.10}$$

$$0 < \lambda_{h_2} = \lambda_{h_2}^{(0)} + \lambda_{h_2}^{(1)}, \tag{II.11}$$

$$0 < \lambda_{k} = \lambda_{k}^{(0)} + \lambda_{k}^{(1)}, \tag{II.12}$$

where the upper indices denote the numbers of the order in loops, and the one loop contributions are given as

$$\lambda_{h_1}^{(1)} = -8|\mu_{11}|^4 F_0(m_{h_1^\pm}, m_{k^{\pm\pm}}), \tag{II.13}$$

$$\lambda_{h_2}^{(1)} = -8|\mu_{22}|^4 F_0(m_{h_2^\pm}, m_{k^{\pm\pm}}), \tag{II.14}$$

$$\lambda_{k}^{(1)} = -4|\mu_{11}|^4 F_0(m_{h_1^\pm}, m_{h_1^\pm}) - 4|\mu_{22}|^4 F_0(m_{h_2^\pm}, m_{h_2^\pm}), \tag{II.15}$$

[3] Another interesting topics is collider searches for a NG boson through invisible channels (subsequent decays from CP even scalars) [95].

with

$$F_0(m_a, m_b) = \frac{1}{(4\pi)^2}\int_0^1 dxdy\delta(x+y-1)\frac{xy}{(xm_a^2+ym_b^2)^2}$$
$$= \begin{cases} \dfrac{1}{(4\pi)^2}\dfrac{m_a^2\left(\log\left(\frac{m_a^2}{m_b^2}\right)-2\right)+m_b^2\left(\log\left(\frac{m_a^2}{m_b^2}\right)+2\right)}{(m_a^2-m_b^2)^3} & (\text{for } m_a \neq m_b), \\ \dfrac{1}{(4\pi)^2}\dfrac{1}{6m_a^4} & (\text{for } m_a = m_b), \end{cases} \tag{II.16}$$

where the form of μ_{11} is shown in Eq. (II.3) and each of m_1 and m_2 in F_0 represents a mass of propagating fields in the loops. We include these constraints in the numerical analysis later. To avoid the global minimum accompanying charge breaking, the following condition should at least be satisfied:

$$|\mu_{22}| < \sqrt{\Lambda}\left[m_\Phi^2 + m_{h_1}^2 + m_{h_2}^2 + m_k^2 + m_\Sigma^2\right]^{1/2}, \quad \Lambda \equiv \sum_{i=\text{all quartic couplings including } \lambda_{11}} \lambda_i, \tag{II.17}$$

where we assume the simplified configuration, $r \equiv |\Phi| = |h_1^+| = |h_2^+| = |k^{++}| = |\Sigma_0|$ and the above inequality comes from the requirement that r does not have a finite nonzero value. The summation is taken over the coefficients of the 17 quartic terms in Eq. (II.2) including $\Sigma_0^* h_1^- h_1^- k^{++}$ and its Hermitian conjugate. When all of these quartic couplings are assumed to take the same value λ, the above condition is rewritten as

$$|\mu_{22}| \lesssim 4\sqrt{\lambda}\left[m_{h_1}^2 + m_{h_2}^2 + m_k^2 + m_\Sigma^2\right]^{1/2}, \tag{II.18}$$

where the contributions via m_Φ^2 and λ_Φ are insignificant and thus neglected.

E. Neutrino mass matrix

A Majorana neutrino mass matrix m_ν is generated at the three loop level via the diagram shown in Fig. 1, which corresponds to the coefficients of the effective operators, $-\frac{1}{2}(m_\nu)_{ab} \times \overline{(\nu_{L_a})^c}\nu_{L_b}$. The form of $(m_\nu)_{ab}$ is evaluated by a straightforward calculation as

$$(m_\nu)_{ab} = \frac{\mu_{11}\mu_{22}}{(4\pi)^6}\sum_{i,j,k=1}^{3}\frac{1}{M_k^4}\left[(y_L)_{ai}m_{\ell_i}(y_R^T)_{ik}(M_{N_k})(y_R)_{kj}m_{\ell_j}(y_L^T)_{jb}\right]$$
$$\times F_1\left(\frac{m_{h_1^+}^2}{M_k^2}, \frac{m_{h_2^+}^2}{M_k^2}, \frac{m_{\ell_i}^2}{M_k^2}, \frac{m_{\ell_j}^2}{M_k^2}, \frac{{M_{N_k}}^2}{M_k^2}, \frac{m_{k^{\pm\pm}}^2}{M_k^2}\right), \tag{II.19}$$

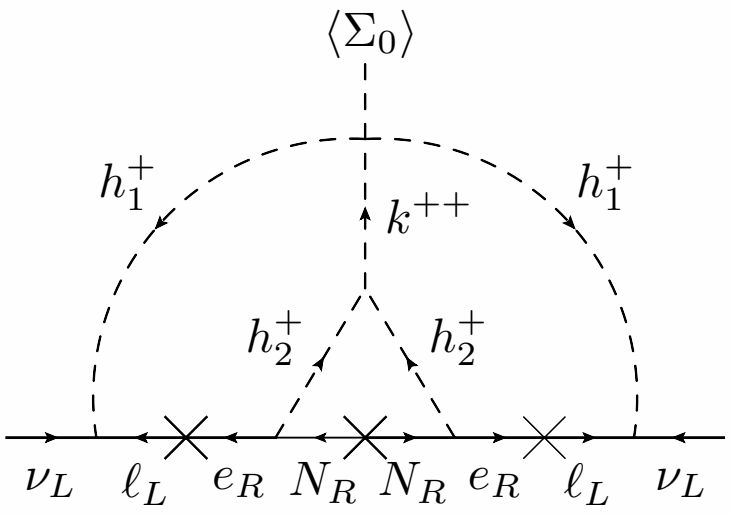

FIG. 1: A schematic description for the radiative generation of neutrino masses.

where the mass scale $M_k = \max[m_{h_1^\pm}, m_{h_2^\pm}, m_{\ell_i}, m_{\ell_j}, M_{N_k}, m_{k^{\pm\pm}}]$ is used for factorizing the loop function F_1 as a dimensionless variable. Here, we take the relationship in masses in our setup, $m_{\ell_i}, m_{\ell_j} < M_{N_k}$, into consideration and then M_k has only the index k. F_1 is symbolically calculated as follows:

$$F_1\left(X_1, X_2, X_3, X_4, X_5, X_6\right) = \int \mathbf{dX} \frac{1}{\Delta_1} \frac{1}{(\Delta_2)^2} \frac{\rho}{(\Delta_3)^2}, \tag{II.20}$$

$$\int \mathbf{dX} = \int_0^1 dx dy dz\, \delta(x+y+z-1) \int_0^1 d\alpha d\beta d\gamma d\delta\, \delta(\alpha+\beta+\gamma+\delta-1) \int_0^1 d\rho d\sigma d\omega\, \delta(\rho+\sigma+\omega-1), \tag{II.21}$$

with

$$\Delta_1 = y(y-1) + z(z-1) + 2yz, \tag{II.22}$$

$$\Delta_2 = (\alpha Y + \delta)^2 - \delta - \alpha Y^2 - \alpha X, \tag{II.23}$$

$$\Delta_3 = \rho A\left(X_1, X_2, X_3, X_5, X_6\right) - \sigma X_4 - \omega X_1, \tag{II.24}$$

$$\begin{aligned} A\left(X_1, X_2, X_3, X_5, X_6\right) = & -\frac{\alpha((x+y)X_2 + zX_5)}{((\alpha Y+\delta)^2 - \delta - \alpha Y^2 - \alpha X)(y(y-1)+z(z-1)+2yz)} \\ & + \frac{\beta X_1 + \gamma X_3 + \delta X_6}{((\alpha Y+\delta)^2 - \delta - \alpha Y^2 - \alpha X)}, \end{aligned} \tag{II.25}$$

$$X = -\left(\frac{y}{y+z}\right)^2 + \frac{y(y-1)}{y(y-1)+z(z-1)+2yz}, \quad Y = \frac{y}{y+z}. \tag{II.26}$$

Here, note that the shape of F_1 is completely the same as that in Ref. [1] except for the content of X_5 in Eq. (II.19).

Neutrino mass eigenstates and their mixings are evaluated by reflecting on similarities to the Zee-Babu model [87]. The structure of the fermion line is similar to the Zee-Babu model [6], that is, a rank two model of the neutrino mass matrix with a massless eigenstate due to the antisymmetricity of y_L. Let us describe the neutrino mass matrix as

$$(m_\nu)_{ab} = (U_{\rm PMNS}\, m_\nu^{\rm diag}\, U_{\rm PMNS}^T)_{ab} \equiv \sum_{i,j=1}^{3} (y_L)_{ai}\omega_{ij}(y_L^T)_{jb}, \tag{II.27}$$

$$\omega_{ij} = \sum_{k=1}^{3} m_{\ell_i}(y_R^T)_{ik}(\zeta_k M_{N_k})(y_R)_{kj} m_{\ell_j}, \tag{II.28}$$

$$\zeta_k = \frac{\mu_{11}\mu_{22}}{(4\pi)^6 M_k^4} F_1\left(\frac{m_{h_1^+}^2}{M_k^2}, \frac{m_{h_2^+}^2}{M_k^2}, 0, 0, \frac{{M_{N_k}}^2}{M_k^2}, \frac{m_{k^{++}}^2}{M_k^2}\right), \tag{II.29}$$

where i, j, k run over 1 to 3, $m_\nu^{\rm diag} \equiv (m_1, m_2, m_3)$ are the neutrino mass eigenvalues, and $U_{\rm PMNS}$ (Pontecorvo-Maki-Nakagawa-Sakata matrix [97, 98]) is the mixing matrix to diagonalize the neutrino mass matrix, which is parametrized as [87]

$$U_{\rm PMNS} = \begin{bmatrix} c_{13}c_{12} & c_{13}s_{12} & s_{13}e^{-i\delta} \\ -c_{23}s_{12} - s_{23}s_{13}c_{12}e^{i\delta} & c_{23}c_{12} - s_{23}s_{13}s_{12}e^{i\delta} & s_{23}c_{13} \\ s_{23}s_{12} - c_{23}s_{13}c_{12}e^{i\delta} & -s_{23}c_{12} - c_{23}s_{13}s_{12}e^{i\delta} & c_{23}c_{13} \end{bmatrix} \begin{bmatrix} 1 & 0 & 0 \\ 0 & e^{i\phi/2} & 0 \\ 0 & 0 & 1 \end{bmatrix}, \tag{II.30}$$

with $c_{ij} \equiv \cos\theta_{ij}$ and $s_{ij} \equiv \sin\theta_{ij}$. δ and ϕ represent the Dirac CP phase and the Majorana one, respectively. Here, we treat the two ratios in F_1, m_{ℓ_i}/M_k and m_{ℓ_j}/M_k as zero values approximately, which means that the loop factor has no dependence on i or j as ζ_k.

Requirements for the observed neutral profiles depend on the ordering of the neutrino masses, which are normal $[m_1\,(=0) < m_2 < m_3]$ or inverted $[m_3\,(=0) < m_1 < m_2]$.[4] When we consider the normal ordering, the following relations should hold for realizing the observed neutrino profiles [87],

$$\begin{aligned}
(y_L)_{13} &= (s_{12}c_{23}/(c_{12}c_{13}) + s_{13}s_{23}e^{-i\delta}/c_{13})(y_L)_{23}, \\
(y_L)_{12} &= (s_{12}s_{23}/(c_{12}c_{13}) - s_{13}c_{23}e^{-i\delta}/c_{13})(y_L)_{23}, \\
\left(\frac{(y_L)_{23}}{2}\right)^2 \omega_{33} &\approx m_3 c_{13}^2 s_{23}^2 + m_2 e^{i\phi}(c_{12}c_{23} - e^{i\delta}s_{12}s_{13}s_{23})^2, \\
\left(\frac{(y_L)_{23}}{2}\right)^2 \omega_{23} &\approx -m_3 c_{13}^2 c_{23}s_{23} + m_2 e^{i\phi}(c_{12}s_{23} + e^{i\delta}c_{23}s_{12}s_{13})(c_{12}c_{23} - e^{i\delta}s_{12}s_{13}s_{23}),
\end{aligned}$$

[4] More details can be given in Ref. [87] for both of the cases.

$$\left(\frac{(y_L)_{23}}{2}\right)^2 \omega_{22} \approx m_3 c_{13}^2 c_{23}^2 + m_2 e^{i\phi}(c_{12}s_{23}+e^{i\delta}c_{23}s_{12}s_{13})^2, \tag{II.31}$$

where we use $m_e \ll m_\mu, m_\tau$. In the case of the inverted neutrino mass hierarchy, the conditions are deformed [87],

$$\begin{aligned}
(y_L)_{13} &= -(c_{13}s_{23}e^{-i\delta}/s_{13})(y_L)_{23}, \\
(y_L)_{12} &= +(c_{13}c_{23}e^{-i\delta}/s_{13})(y_L)_{23}, \\
\left(\frac{(y_L)_{23}}{2}\right)^2 \omega_{33} &\approx m_1(c_{23}s_{12} + e^{i\delta}c_{12}s_{13}s_{23})^2 + m_2 e^{i\phi}(c_{12}c_{23} - e^{i\delta}s_{12}s_{13}s_{23})^2, \\
\left(\frac{(y_L)_{23}}{2}\right)^2 \omega_{23} &\approx m_1(s_{12}s_{23} - e^{i\delta}c_{12}c_{23}s_{13})(c_{23}s_{12} + e^{i\delta}c_{12}s_{13}s_{23}) \\
&\quad + m_2 e^{i\phi}(c_{12}s_{23} + e^{i\delta}c_{23}s_{12}s_{13})(c_{12}c_{23} - e^{i\delta}s_{12}s_{13}s_{23}), \\
\left(\frac{(y_L)_{23}}{2}\right)^2 \omega_{22} &\approx m_1(s_{12}s_{23} - e^{+i\delta}c_{12}c_{23}s_{13})^2 + m_2 e^{i\phi}(c_{12}s_{23}+e^{i\delta}c_{23}s_{12}s_{13})^2.
\end{aligned} \tag{II.32}$$

In the numerical analysis in the following Sec. III B, we adopt the latest values of θ_{12}, θ_{23}, θ_{13}, Δm^2_{21} and $\Delta m^2_{3\ell}$ ($\ell = 1$ for the normal hierarchy and $\ell = 2$ for the inverted one) found in Ref. [99]. The two CP-violating phases δ and ϕ are treated as free parameters.[5]

F. Lepton flavor violations and the universality of charged currents

In the present model, owing to interactions containing charged scalars, new contributions to several lepton-flavor-violating processes are found at the tree or the one loop level. Also, universalities of charged currents are threatened by the vertices. Some of them are very similar to the case of the Zee-Babu model discussed, *e.g.*, in Ref. [81], while situations are changed in the others. Here, we briefly summarize important points:

- $\ell_i \to \ell_j \nu\bar{\nu}$: like in the Zee-Babu model, the processes receive additional contributions that are never found in the SM via the exchange of the singly charged scalar coupling to the charged leptons $h_1^\pm$, which have an influence on the value of the Fermi constant via charged-lepton decay. If the masses of the right-hand neutrinos are small, there is

[5] The best fit values are as follows: $\sin^2\theta_{12} = 0.304$, $\sin^2\theta_{23} = 0.452$, $\sin^2\theta_{13} = 0.0218$, $\Delta m^2_{21} = 7.50 \times 10^{-5}\,\mathrm{eV}^2$, $\Delta m^2_{31} = +2.457 \times 10^{-3}\,\mathrm{eV}^2$ (in the normal hierarchy); $\sin^2\theta_{12} = 0.304$, $\sin^2\theta_{23} = 0.579$, $\sin^2\theta_{13} = 0.0219$, $\Delta m^2_{21} = 7.50 \times 10^{-5}\,\mathrm{eV}^2$, $\Delta m^2_{32} = -2.449 \times 10^{-3}\,\mathrm{eV}^2$ (in the inverted hierarchy) [99].

a possibility that the channels $\ell_i \to \ell_j N_1 \bar{N}_1$ via the exchange of $h_2^\pm$ are open and they fake contributions to $\ell_i \to \ell_j \nu \bar{\nu}$. In this paper, we do not consider such a light N_1. Then, we simply ignore this effect in the following analysis part.

- $\ell_i^- \to \ell_f^- \gamma$: like in the Zee-Babu model, these decay sequences (when $m_{\ell_i^-} > m_{\ell_f^-}$) are radiatively generated at the one loop level via the diagrams containing charged scalars which the photon couples to. In these processes, both of the interactions, $\bar{L}^c_{L_i} L_{L_j} h_1^+$ and $\bar{N}_{R_i} e^c_{R_j} h_2^-$ (also with their Hermitian conjugations included) make nonzero contributions to the decay widths. The doubly charged scalar $k^{\pm\pm}$ has no contribution at the one loop level due to the absence of tree-level interactions with the charged leptons.

- $\ell_i^- \to \ell_j^+ \ell_k^- \ell_l^-$: being different from the Zee-Babu model, absence of direct interactions between the charged leptons and the doubly charged scalar $k^{\pm\pm}$ generates the situation that these processes are induced at the one loop level. Two types of box diagrams contributing to the processes are there: containing (i) $\bar{L}^c_{L_i} L_{L_j} h_1^+$ interactions; and containing (ii) $\bar{N}_{R_i} e^c_{R_j} h_2^-$ ones (where their Hermitian conjugations are also included), while two types of photon and Z penguin diagrams are also generated. Here, the contribution from the penguins is directory related to the dipole diagrams of $\ell_i^- \to \ell_f^- \gamma$ in the language of branching ratios, *e.g.*, when we consider $\mu \to 3e$ [100–102] as

$$\mathrm{Br}(\mu \to 3e) \simeq \frac{\alpha_{\mathrm{EM}}}{3\pi} \left(\log \left(\frac{m_\mu^2}{m_e^2} \right) - \frac{11}{4} \right) \mathrm{Br}(\mu \to e\gamma), \tag{II.33}$$

  where α_{EM} is the electromagnetic fine structure constant and the penguin-type contributions to $\mu \to 3e$ are suppressed compared with those to $\mu \to e\gamma$. Since the experimental bounds on $\ell_i^- \to \ell_f^- \gamma$ and $\ell_i^- \to \ell_j^+ \ell_k^- \ell_l^-$ are roughly comparable, we simply ignore the contributions from the penguin-type diagrams in the calculation of the constraints in this category.

Now we show the explicit forms of constraints on the present model. We recast the results of the analysis on the Zee-Babu model in Ref. [87] for our case, where the three $\ell \to \ell\gamma$ processes ($\mu^- \to e^-\gamma$, $\tau^- \to e^-\gamma$, $\tau^- \to \mu^-\gamma$), the four types of gauge universalities (lepton/hadron, μ/e, τ/μ, τ/e), and the seven $\ell \to 3\ell$ processes ($\mu^- \to e^+e^-e^-$, $\tau^- \to e^+e^-e^-$, $\tau^- \to e^+e^-\mu^-$, $\tau^- \to e^+\mu^-\mu^-$, $\tau^- \to \mu^+e^-e^-$, $\tau^- \to \mu^+e^-\mu^-$, $\tau^- \to \mu^+\mu^-\mu^-$) are included.

Process	(i,f)	Experimental bounds (90% C.L.)	C_{if}
$\mu^- \to e^-\gamma$	$(2,1)$	$\mathrm{Br}(\mu \to e\gamma) < 5.7 \times 10^{-13}$	1.6×10^{-6}
$\tau^- \to e^-\gamma$	$(3,1)$	$\mathrm{Br}(\tau \to e\gamma) < 3.3 \times 10^{-8}$	0.52
$\tau^- \to \mu^-\gamma$	$(3,2)$	$\mathrm{Br}(\tau \to \mu\gamma) < 4.4 \times 10^{-8}$	0.7

TABLE II: Summary of the coefficient C_{if} in $\ell \to \ell\gamma$ processes and experimental data used in the analysis in [87].

Type of universality	Experimental bounds (90% C.L.)
Lepton/hadron universality	$\sum_{q=d,s,b} \lvert V_{uq}^{\mathrm{exp}} \rvert = 0.9999 \pm 0.0006$
μ/e universality	$G_\mu^{\mathrm{exp}}/G_e^{\mathrm{exp}} = 1.0010 \pm 0.0009$
τ/μ universality	$G_\tau^{\mathrm{exp}}/G_\mu^{\mathrm{exp}} = 0.9998 \pm 0.0013$
τ/e universality	$G_\tau^{\mathrm{exp}}/G_e^{\mathrm{exp}} = 1.0034 \pm 0.0015$

TABLE III: Summary of the experimental data on universality of charged currents used in the analysis in [87].

- $\ell_i^- \to \ell_f^-\gamma$ processes: in this case, the result of recasting is

$$\frac{\left|\sum_{a=1}^3 \left[(y_L^\dagger)_{af}(y_L)_{ia}\right]^2 \left(I_{1,a}I_{2,a} + I_{1,a}^2\right) + \sum_{a=1}^3 \left[(y_R)_{af}(y_R^\dagger)_{ia}\right]^2 \left(I'_{1,a}I'_{2,a} + {I'_{1,a}}^2\right)\right|}{16 m_{h_1^\pm}^4 \left|\sum_{a=1}^3 \left(I_{1,a}I_{2,a} + I_{1,a}^2\right)\right|} < \frac{C_{if}}{\mathrm{TeV}^4}, \tag{II.34}$$

with the loop functions

$$I_{1,a} = \frac{1}{(4\pi)^2}\int_0^1 dx \int_0^{1-x} dy\, \frac{x(2x-1)}{(x+y)m_{h_1^\pm}^2 + (1-x-y)m_{\nu_a}^2} \simeq -\frac{1}{(4\pi)^2}\frac{1}{36 m_{h_1^\pm}^2}, \tag{II.35}$$

$$I_{2,a} = \frac{1}{(4\pi)^2}\int_0^1 dx \int_0^{1-x} dy\, \frac{x(2y-1)}{(x+y)m_{h_1^\pm}^2 + (1-x-y)m_{\nu_a}^2} \simeq -\frac{1}{(4\pi)^2}\frac{5}{36 m_{h_1^\pm}^2}, \tag{II.36}$$

$$I'_{1,a} = \frac{1}{(4\pi)^2}\int_0^1 dx \int_0^{1-x} dy\, \frac{x(2x-1)}{(x+y)m_{h_2^\pm}^2 + (1-x-y)M_{N_a}^2}, \tag{II.37}$$

$$I'_{2,a} = \frac{1}{(4\pi)^2}\int_0^1 dx \int_0^{1-x} dy\, \frac{x(2y-1)}{(x+y)m_{h_2^\pm}^2 + (1-x-y)M_{N_a}^2}, \tag{II.38}$$

where we use $m_{\nu_a} \simeq 0$. Here, we treat the final-state lepton ℓ_f^- as a massless particle. Concrete forms of the integrals are summarized in Appendix A. The dimensionless coefficient C_{if} representing the digits in [87] (before recasting) are summarized in

Process	(i,j,k,l)	Experimental bounds (90% C.L.)	A_{ijkl}
$\mu^- \to e^+e^-e^-$	$(2,1,1,1)$	$\mathrm{Br} < 1.0 \times 10^{-12}$	2.3×10^{-5}
$\tau^- \to e^+e^-e^-$	$(3,1,1,1)$	$\mathrm{Br} < 2.7 \times 10^{-8}$	0.009
$\tau^- \to e^+e^-\mu^-$	$(3,1,1,2)$	$\mathrm{Br} < 1.8 \times 10^{-8}$	0.005
$\tau^- \to e^+\mu^-\mu^-$	$(3,1,2,2)$	$\mathrm{Br} < 1.7 \times 10^{-8}$	0.007
$\tau^- \to \mu^+e^-e^-$	$(3,2,1,1)$	$\mathrm{Br} < 1.5 \times 10^{-8}$	0.007
$\tau^- \to \mu^+e^-\mu^-$	$(3,2,1,2)$	$\mathrm{Br} < 2.7 \times 10^{-8}$	0.007
$\tau^- \to \mu^+\mu^-\mu^-$	$(3,2,2,2)$	$\mathrm{Br} < 2.1 \times 10^{-8}$	0.008

TABLE IV: Summary of the coefficient A_{ijkl} in $\ell \to 3\ell$ processes and experimental data used in the analysis in [87].

Table II. The factor 16 comes from the difference in the coupling convention of the interaction $\bar{L}^c_{L_i} L_{L_j} h_1^+$ ($\bar{L}^c_{L_i} L_{L_j} h^+$ in the Zee-Babu model). These decay processes are one loop induced ones in both of the models, and thus the loop factor $1/(4\pi)^2$ in the integrals is canceled out in the final form in Eq. (II.34).

- Gauge coupling universalities: in this category, recasting is just straightforward by the replacement $h^\pm \to h_1^\pm$,

$$\begin{aligned}
\left|\frac{(y_L)_{12}}{2}\right|^2 &< 0.007 \left(\frac{m_{h_1^\pm}}{\mathrm{TeV}}\right)^2 \quad \text{(lepton/hadron universality)},\\
\left|\left|\frac{(y_L)_{23}}{2}\right|^2 - \left|\frac{(y_L)_{13}}{2}\right|^2\right| &< 0.024 \left(\frac{m_{h_1^\pm}}{\mathrm{TeV}}\right)^2 \quad (\mu/e \text{ universality}),\\
\left|\left|\frac{(y_L)_{13}}{2}\right|^2 - \left|\frac{(y_L)_{12}}{2}\right|^2\right| &< 0.035 \left(\frac{m_{h_1^\pm}}{\mathrm{TeV}}\right)^2 \quad (\tau/\mu \text{ universality}),\\
\left|\left|\frac{(y_L)_{23}}{2}\right|^2 - \left|\frac{(y_L)_{12}}{2}\right|^2\right| &< 0.04 \left(\frac{m_{h_1^\pm}}{\mathrm{TeV}}\right)^2 \quad (\tau/e \text{ universality}).
\end{aligned} \tag{II.39}$$

The corresponding experimental bounds are summarized in Table III.

- $\ell \to 3\ell$ processes: all of the cases are summarized symbolically as

$$\frac{1}{4}\left| |A_\nu + B_\nu|^2 + |A_N + B_N|^2 - 2\,\mathrm{Re}\,[A_N C_N^*] - 2\,\mathrm{Re}\,[B_N C_N^*] + \frac{1}{2}|C_N|^2 \right|^{1/2} < \frac{A_{ijkl}}{\mathrm{TeV}^2}, \tag{II.40}$$

with the effective couplings

$$A_\nu = (y_L y_L^\dagger)_{ik}(y_L y_L^\dagger)_{jl}\, J_{1,0}, \tag{II.41}$$

$$B_\nu = (y_L y_L^\dagger)_{il}(y_L y_L^\dagger)_{jk}\, J_{1,0}, \tag{II.42}$$

$$A_N = \sum_{a,b=1}^{3} (y_R)_{al}(y_R)_{bk}(y_R^\dagger)_{ja}(y_R^\dagger)_{ib}\, J_{1,ab}, \tag{II.43}$$

$$B_N = \sum_{a,b=1}^{3} (y_R)_{al}(y_R)_{bk}(y_R^\dagger)_{jb}(y_R^\dagger)_{ia}\, J_{1,ab}, \tag{II.44}$$

$$C_N = 2\sum_{a,b=1}^{3} (y_R)_{al}(y_R)_{ak}(y_R^\dagger)_{jb}(y_R^\dagger)_{ib} M_{N_a} M_{N_b} J_{2,ab}. \tag{II.45}$$

The loop functions $J_{1,ab}$ and $J_{2,ab}$ are given as

$$J_{1,ab} = \frac{1}{(4\pi)^2}\int_0^1 dx \int_0^{1-x} dy\, \frac{1-x-y}{xM_{N_a}^2 + yM_{N_b}^2 + (1-x-y)m_{h_2^\pm}^2}, \tag{II.46}$$

$$J_{2,ab} = \frac{1}{(4\pi)^2}\int_0^1 dx \int_0^{1-x} dy\, \frac{1-x-y}{\left[xM_{N_a}^2 + yM_{N_b}^2 + (1-x-y)m_{h_2^\pm}^2\right]^2}, \tag{II.47}$$

where the form of $J_{1,0}$ is obtained by the replacements $M_{N_a} \to m_{\nu_a}(\simeq 0)$, $M_{N_b} \to m_{\nu_b}(\simeq 0)$ and $m_{h_2^\pm} \to m_{h_1^\pm}$ as

$$J_{1,0} \simeq \frac{1}{2}\frac{1}{(4\pi)^2}\frac{1}{m_{h_1^\pm}^2}. \tag{II.48}$$

Also in this calculation, we treat the final-state leptons ℓ_j^+, ℓ_k^- and ℓ_l^- as massless particles. Other concrete forms of the integrals are summarized in Appendix A. Here, the dimensionless valuables A_{ijkl} indicate the numerical values (in the analysis in [87] before recasting) and their concrete values are summarized in Table IV. The factor $1/4$ originates from recasting. The loop suppression factor $1/(4\pi)^2$ should appear in Eq. (II.40) since these processes are generated at the tree level in the original Zee-Babu model.

Finally, we briefly have a discussion on the LFV via $k^{\pm\pm}$ exchange in our model. When we focus on the LFV process accompanying two neutrinos, $\ell^- \to k^{--}\ell^+ \to 2(h_1^-)^* + \ell^+ \to (2\ell^- + 2\nu) + \ell^+$, where the first step is one loop induced and the two h_1^- as intermediate states are usually off shell since the mass of h_1^- is bounded from below, where $m_{h_1^\pm}$ should be more than a few TeV; see Sec. III for details. The order of the loops is the same as that

of $\ell \to 3\ell$. But, the off shellness suppresses the decay width of this LFV process. Therefore we can simply ignore this possibility.

III. VALID PARAMETER REGION WITH NEUTRINO SECTOR

A. Form of y_R

Different from the Zee-Babu model, y_R is not a symmetric matrix in general but $y_R^T(\zeta M_N)\, y_R\, (\equiv Y_R)$ is symmetric one. Hence, we can utilize fitting relations in the Zee-Babu model with modifications. Here, we adopt the following forms in y_R [and in y_N as shown in Eq. (II.4)] for simplicity,

$$y_R = \begin{bmatrix} * & * & * \\ * & a & b \\ * & b & c \end{bmatrix}, \quad M_N = \mathrm{diag}\,(M_{N_1}, M_{N_2}, M_{N_3}), \tag{III.1}$$

where a, b, c are arbitrary complex numbers. The correspondence to the factors ω_{ij} in Eq. (II.28) is as follows:

$$\omega_{ij} = m_{\ell_i} (Y_R)_{ij} m_{\ell_j}. \tag{III.2}$$

Here, because of the mass hierarchy of the charged leptons $m_{\ell_1} \ll m_{\ell_2} < m_{\ell_3}$, the terms in ω_{ij} including m_{ℓ_1} are negligible. Combining this issue with the hierarchy assumed in the right-hand neutrinos $M_{N_1} < M_{N_2} < M_{N_3}$, we conclude that the elements of y_R expressed by $*$ in Eq. (III.1) do not affect the values of ω_{ij} significantly. Therefore in the following analysis, we only consider the couplings a, b, c of y_R in fitting the neutrino profiles.

Now, we rewrite the relations in Eq. (III.2) as follows:

$$\begin{aligned} \frac{\omega_{22}}{m_{\ell_2}^2} &= (Y_R)_{22} \simeq \left[a^2(\zeta_2 M_{N_2}) + b^2(\zeta_3 M_{N_3})\right], \\ \frac{\omega_{23}}{m_{\ell_2} m_{\ell_3}} &= (Y_R)_{23} \simeq \left[ab\,(\zeta_2 M_{N_2}) + bc\,(\zeta_3 M_{N_3})\right], \\ \frac{\omega_{33}}{m_{\ell_3}^2} &= (Y_R)_{33} \simeq \left[b^2(\zeta_2 M_{N_2}) + c^2(\zeta_3 M_{N_3})\right]. \end{aligned} \tag{III.3}$$

As shown in Eqs. (II.31)–(II.32), when we fix the values of $(y_L)_{23}$, δ and ϕ, the values of ω_{22}, ω_{23}, ω_{33} [and also $(y_L)_{12}$, $(y_L)_{13}$] are automatically determined through the relations. In each scanning in the following section, we pick up a solution on a, b, c of the above simultaneous equations.

B. Parameter scanning

Adopting the structure of y_R in the previous subsection, we execute parameter scans to search for consistent regions in the parameter space. In this model, $k^{\pm\pm}$ does not contribute to the processes with LFV significantly. Thus, we consider the two possibilities $m_{k^{\pm\pm}} = 250$ and 500 GeV, while the other two singly charged scalars $h_{1^\pm}, h_{2^\pm}$ have a few TeV masses. Here, we select the four choices: $m_{h_1^\pm} = m_{h_2^\pm} = 3$, 3.5, 4, and 4.8 TeV. For brevity, we fix the three right-hand neutrinos as follows: $M_{N_1} = m_h/2$, $M_{N_2} = 5\,\text{TeV}$ and $M_{N_3} = 10\,\text{TeV}$, where we mention that N_1 is a "Higgs-portal" dark matter candidate. The mass is assumed to be around the 125 GeV Higgs resonant region. Detailed discussion on this topic is found in Sec. V.

We mention that compliance with the relations in the case of the normal hierarchy in Eq. (II.31) or the inverted hierarchy in Eq. (II.32) leads to the situation that only the parameters μ_{11}, μ_{22}, δ, ϕ, $(y_L)_{23}$ are free to be chosen (in addition to the masses of particles that we fixed in the above paragraph). Note that the five matrix elements of y_R, namely $(y_R)_{11}$, $(y_R)_{12}$, $(y_R)_{13}$, $(y_R)_{21}$, and $(y_R)_{31}$, are ineffective in the determination of the active neutrino profiles, while their nonzeroness possibly modifies the strengths of the lepton-flavor-violating processes significantly. Then we consider nonzero values in the five couplings for the sake of completeness. In each scanning, we randomly select values of the ten parameters within the corresponding ranges

$$\begin{aligned} &\mu_{12} = \mu_{22}\ (\equiv \mu) \in [1\,\text{TeV}, 20\,\text{TeV}], \quad \delta \in [0, 2\pi], \quad \phi \in [0, 2\pi], \quad (y_L)_{23} \in [-1, 1], \\ &(y_R)_{ij} \in [-0.01, -0.1] \cup [0.01, 0.1] \quad \Big(\text{for } (i,j) = (1,1), (1,2), (1,3), (2,1), (3,1)\Big). \end{aligned} \tag{III.4}$$

Our definition of an allowed point is a set of parameters where all the following requirements are satisfied:

- Observed values in masses and mixings of the three active neutrinos are generated. As we mentioned above, realization of this requirement is equal to the compliance with the relations in Eq. (II.31) or (II.32).

- Predictions for LFVs do not exceed the bounds shown in Tables II ($\ell \to \ell\gamma$), III (gauge universalities), and IV ($\ell \to 3\ell$). Concretely, evading bounds corresponds to meeting the inequalities in Eqs. (II.34) and (II.39)–(II.40), respectively.

$m_{k^{\pm\pm}}$	$(m_{h_1^\pm}, m_{h_2^\pm})$	$F_1^{(\zeta_2)}$	$F_1^{(\zeta_3)}$	Number of allowed points
500 GeV	(4.8 TeV, 4.8 TeV)	−1.16818	−11.5428	2804
	(4.0 TeV, 4.0 TeV)	−2.14198	−20.0287	422
	(3.5 TeV, 3.5 TeV)	−3.30195	−29.6525	89
	(3.0 TeV, 3.0 TeV)	−5.37518	−46.0932	16
250 GeV	(4.8 TeV, 4.8 TeV)	−1.21466	−11.9695	1644
	(4.0 TeV, 4.0 TeV)	−2.24746	−20.9444	190
	(3.5 TeV, 3.5 TeV)	−3.49141	−31.2321	31
	(3.0 TeV, 3.0 TeV)	−5.74153	−49.0141	2

TABLE V: The numbers of consistent points in the normal hierarchy obtained by parameter scanning. $F_1^{(\zeta_2)}$ and $F_1^{(\zeta_3)}$ are the loop functions in ζ_2 and ζ_3 shown in Eq. (II.29), respectively. Kindly refer to the main body of this subsection for details of this scanning.

- Fulfilling the requirements on vacuum stability in Eqs. (II.10)–(II.12) and (II.18). In the last condition, we adopt the following modified form with physical masses,

$$|\mu_{22}| \lesssim 4\sqrt{\lambda}\left[m_{h_1^\pm}^2 + m_{h_2^\pm}^2 + m_{k^{\pm\pm}}^2\right]^{1/2}, \tag{III.5}$$

  where we simply change the parameters m_{h_1}, m_{h_2}, m_k to their physical masses and ignore the mass parameter m_Σ. The value of the right-hand side would be near the original one and it would be useful for roughly estimating this type of bound. In the following analysis, we adopt the initial conditions for the quartic couplings,

$$\lambda_{h_1}^{(0)} = \lambda_{h_2}^{(0)} = \lambda_k^{(0)} = 4\pi, \quad \lambda = 4\pi. \tag{III.6}$$

- Ensuring perturbativity, all the couplings should be equal to or less than 4π.

Our result in the normal hierarchy is summarized in Table V. In each of the eight combinations of the charged scalar masses, we randomly scan 10^5 points in the ten parameters, where the range we consider is shown in Eq. (III.4). Apart from the previous work [1], the result says that the mass of the doubly charged scalar can be light around a few hundred GeV, whereas the other two singly charged ones should be heavy (at least) around a few TeV. In this scenario, it is very hard to produce $h_1^\pm$ and $h_2^\pm$ in colliders. On the other hand,

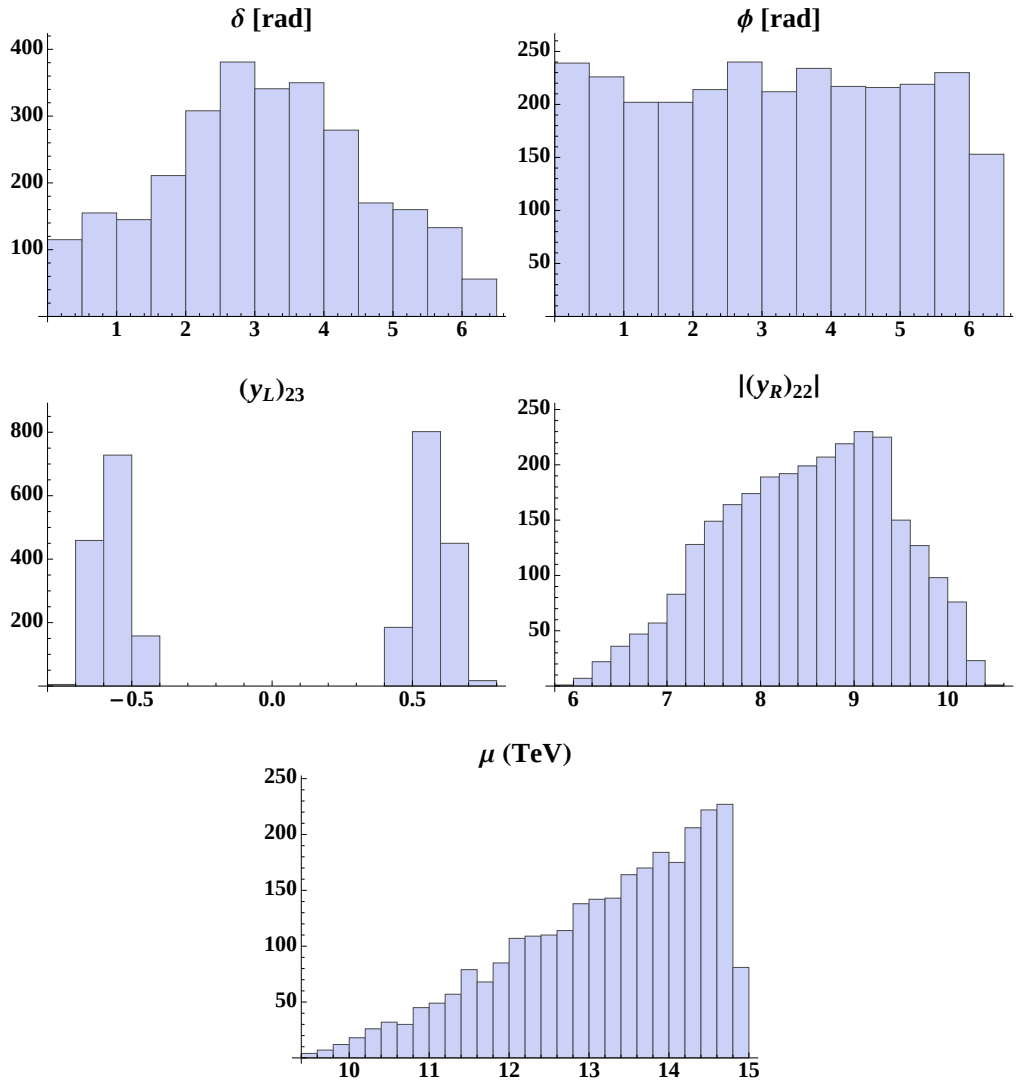

FIG. 2: Histograms showing distributions of δ, ϕ, $(y_L)_{23}$, $|(y_R)_{22}|$ and μ of the result of a scanning with the charged scalar masses $m_{k^{\pm\pm}} = 500\,\text{GeV}$, $m_{h_1^\pm} = m_{h_2^\pm} = 4.8\,\text{TeV}$. The total number of the consistent data points is 2804.

detecting $k^{\pm\pm}$ could be a reasonable option for probing this model in present and future collider experiments.[6]

Next, we look into properties of the parameters in the allowed region. Here, we only show

[6] Lower bounds at 95% CL on $m_{k^{\pm\pm}}$ via 8 TeV data were provided by the ATLAS group in Ref. [103] as 374 GeV, 402 GeV, 438 GeV when assuming a 100% branching ratio to $e^\pm e^\pm$, $e^\pm \mu^\pm$, $\mu^\pm \mu^\pm$ pairs, respectively. In our model, the decay sequence $k^{\pm\pm} \to \ell^\pm \ell^\pm$ is one-loop induced and many parameters contribute. In this paper, we skip to have detailed discussions on prospects in colliders.

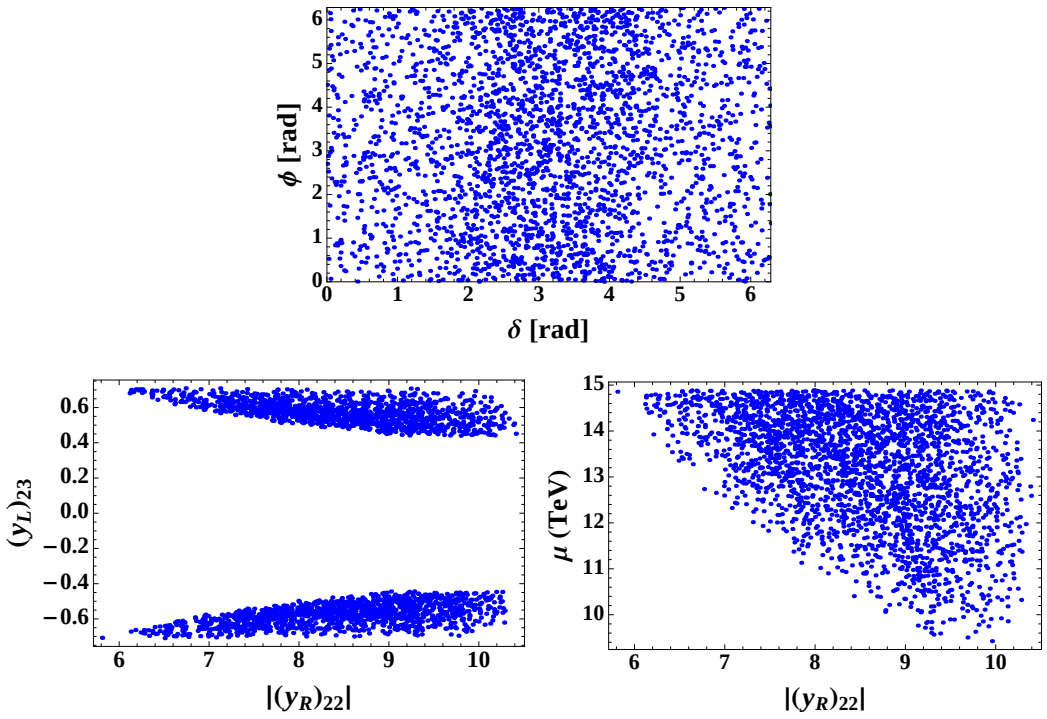

FIG. 3: Correlations between ϕ and δ, $(y_L)_{23}$ and $|(y_R)_{22}|$, and μ and $|(y_R)_{22}|$ are shown. The data set is the same as in Fig. 2.

the case of $m_{k^{\pm\pm}} = 500\,\mathrm{GeV}$, $m_{h_1^\pm} = m_{h_2^\pm} = 4.8\,\mathrm{TeV}$ as an example, where we checked that other cases are not so different. In Fig. 2, we display the distributions of δ, ϕ, $(y_L)_{23}$, $|(y_R)_{22}|$ and μ based on 2804 data points of the allowed region as histograms.[7] The correlations between ϕ and δ, $(y_L)_{23}$ and $|(y_R)_{22}|$, and μ and $|(y_R)_{22}|$ are also shown in Fig. 3. In the present three loop scenario, the loop factor $1/(4\pi)^6$ in the neutrino masses tends to suppress the realized masses very much. Thus, at least a part of the parameters related with the masses would be sufficiently large. In the following, we investigate details.

- We can see that this model could give some preference to δ around π. On the other hand, δ not around π is also realized. Few trends are seen in the distribution of ϕ.

- A typical digit of the absolute value of $(y_L)_{23}$ is in $0.5 \sim 0.6$, which would be greater compared with other radiative neutrino models in one or two loop level. Since $|\omega_{22}| \simeq$

[7] The value of $(y_R)_{22}$ is complex in general obtained as a part of a solution of the simultaneous equations in Eq. (III.3).

$|\omega_{23}| \simeq |\omega_{33}|$, the other two nonzero components of y_L, $(y_L)_{12}$ and $(y_L)_{13}$, tend to have almost the same order of magnitude.

- Like the Zee-Babu model, via the relation $|\omega_{22}| \simeq |\omega_{23}| \simeq |\omega_{33}|$, the three components of the effective symmetric Yukawa couplings Y_R meet the definite hierarchy,

$$|(Y_R)_{33}| : |(Y_R)_{23}| : |(Y_R)_{22}| \sim \frac{m_\mu^2}{m_\tau^2} : \frac{m_\mu}{m_\tau} : 1, \tag{III.7}$$

  which means that the original $|(y_R)_{22}|$ tends to hold a significantly large value. The peak of the distribution is around 9, which is still rather small compared with the perturbative upper bound 4π. Because of this characteristic, the masses of the singly charged scalars $m_{h_1^\pm}$ and $m_{h_2^\pm}$ should be greater than around 3 TeV to circumvent the bounds.

- The common coefficients of the trilinear terms μ should be large at around $14 \sim 15$ TeV to compensate for the suppression factor in the neutrino masses. From the perturbativity in the couplings λ_{11} in the form of the trilinear coupling μ_{11} in Eq. (II.3) and y_N found in the masses of the right-hand neutrinos in Eq. (II.4), v' cannot be so small. A reasonable value of v' is $\mathcal{O}(1)$ TeV.

Finally, we briefly comment on the possibility with the inverted mass hierarchy. In our model, like the Zee-Babu model, the components of the active neutrino mass matrix $(m_\nu)_{ab}$ contain the charged lepton masses, and also the Majorana masses with the assumed mass hierarchy $M_{N_1} < M_{N_2} < M_{N_3}$. Then the normal hierarchy would be preferable. Within our search among 10^5 points in the inverted case, even in the choice of $(m_{k^{\pm\pm}}, m_{h_1^\pm}, m_{h_2^\pm}) = (500\,\text{GeV}, 4.8\,\text{TeV}, 4.8\,\text{TeV})$, no solution is found.

IV. CONSTRAINT FROM LHC HIGGS SEARCH

In this part, we evaluate constraints on the parameter space of scalars in this model by use of the latest results of LHC Higgs searches by the ATLAS and CMS experiment groups. First, we describe the method we use for global analysis. Like in the papers [104–106], we adopt the following form of signal strength of the single Higgs production channel with the subsequent Higgs decay to the particles f,

$$\mu_f = \frac{\sigma_{\text{total}}}{\sigma_{\text{total}}^{\text{SM}}} \times \frac{\text{Br}_{h\to f}}{\text{Br}_{h\to f}^{\text{SM}}}, \tag{IV.1}$$

Process	ATLAS	CMS	Reference
$h \to \gamma\gamma$	$1.17^{+0.27}_{-0.27}$	1.12 ± 0.24	[107, 112]
$h \to ZZ^* \to 4\ell$	$1.44^{+0.40}_{-0.33}$	1.00 ± 0.29	[108, 112]
$h \to WW^* \to \ell\nu\ell\nu$	$1.09^{+0.23}_{-0.21}$	0.83 ± 0.21	[109, 112]
$h \to b\bar{b}$	$0.5^{+0.4}_{-0.4}$	0.84 ± 0.44	[110, 112]
$h \to \tau\bar{\tau}$	$1.4^{+0.4}_{-0.4}$	0.91 ± 0.28	[111, 112]

TABLE VI: Summary of the latest LHC Higgs search data as (combined) signal strengths in the five Higgs decay patterns ($h \to \gamma\gamma, h \to ZZ^* \to 4\ell, h \to WW^* \to \ell\nu\ell\nu, h \to b\bar{b}, h \to \tau\bar{\tau}$). The analyses are based on the data sets accumulated in the LHC first run, whose details of the ATLAS and the CMS are 4.5 – $4.7\,\mathrm{fb}^{-1}\,(7\,\mathrm{TeV}) + 20.3\,\mathrm{fb}^{-1}\,(8\,\mathrm{TeV})$, $5.1\,\mathrm{fb}^{-1}\,(7\,\mathrm{TeV}) + 19.7\,\mathrm{fb}^{-1}\,(8\,\mathrm{TeV})$, respectively.

where σ_{total} ($\sigma^{\mathrm{SM}}_{\mathrm{total}}$) represents the total production cross section of a Higgs boson in this model (SM), respectively. The Higgs branching ratios to the particles f of the SM and this model are discriminated by having or not having the superscript SM.

Here, note that in our scenario, the observed Higgs boson is a mixture of the $SU(2)_L$ doublet Φ and the singlet Σ_0 as shown in Eq. (II.8) and no additional colored particle is introduced, which means the absence of new contributions to the Higgs production via the gluon fusion process. Since the SM gauge bosons and quarks do not couple to Σ_0, the ratio of the total cross sections is easily calculated as

$$\frac{\sigma_{\mathrm{total}}}{\sigma^{\mathrm{SM}}_{\mathrm{total}}} = \cos^2\alpha. \tag{IV.2}$$

Whereas, evaluating the ratio of the branding ratios is rather complicated. First, we look at the following decomposition,

$$\frac{\mathrm{Br}_{h\to f}}{\mathrm{Br}^{\mathrm{SM}}_{h\to f}} = \left(\frac{\Gamma_h}{\Gamma^{\mathrm{SM}}_h}\right)^{-1} \times \frac{\Gamma_{h\to f}}{\Gamma^{\mathrm{SM}}_{h\to f}}, \tag{IV.3}$$

where $\Gamma^{(\mathrm{SM})}_h$ represents the corresponding Higgs total width. In the Higgs decay, the presence of the charged scalars in our model ($h^\pm_1, h^\pm_2, k^{\pm\pm}$) also modifies the partial decay widths of the photon-associated decay processes, $h \to \gamma\gamma$ and $h \to Z\gamma$, in addition to the doublet-singlet mixing effect. As we discussed in Sec. III B, the two singly charged scalars tend to be very massive at around a few TeV at least. In such a situation, we can completely neglect

the effect via the two particles and then only the contribution from $k^{\pm\pm}$ is included as a loop effect in the following part.

The ratio of the total widths is rewritten as follows:

$$\frac{\Gamma_h}{\Gamma_h^{\rm SM}} = {\rm Br}^{\rm SM}_{h\to {\rm SM\,others}} \times \frac{\Gamma_{h\to {\rm SM\,others}}}{\Gamma^{\rm SM}_{h\to {\rm SM\,others}}} + {\rm Br}^{\rm SM}_{h\to\gamma\gamma} \times \frac{\Gamma_{h\to\gamma\gamma}}{\Gamma^{\rm SM}_{h\to\gamma\gamma}} + {\rm Br}^{\rm SM}_{h\to Z\gamma} \times \frac{\Gamma_{h\to Z\gamma}}{\Gamma^{\rm SM}_{h\to Z\gamma}} + \frac{\Gamma_{h\to {\rm inv}}}{\Gamma_h^{\rm SM}}, \tag{IV.4}$$

where $\Gamma_{h\to {\rm inv}}$ expresses the Higgs partial decay width to invisible pairs, which is written as

$$\Gamma_{h\to {\rm inv}} = \Gamma_{h\to GG} + \Gamma_{h\to N_{R_1}\bar{N}_{R_1}}. \tag{IV.5}$$

Concrete forms of partial decay width are summarized in Appendix B.

${\rm Br}^{\rm SM}_{h\to {\rm SM\,others}}$ can be described as $1 - {\rm Br}^{\rm SM}_{h\to\gamma\gamma} - {\rm Br}^{\rm SM}_{h\to Z\gamma}$ very precisely. In the following analysis, we use the values ${\rm Br}^{\rm SM}_{h\to\gamma\gamma} = 2.28\times10^{-3}$, ${\rm Br}^{\rm SM}_{h\to Z\gamma} = 1.54\times10^{-3}$ and $\Gamma_h^{\rm SM} = 4.07\,{\rm MeV}$ in $m_h = 125\,{\rm GeV}$ reported by the LHC Higgs Cross Section Working Group [113]. The ratios of the partial decay widths are described with the help of the formulas for $h\to\gamma\gamma$ and $h\to Z\gamma$ in Refs. [114–118] as

$$\frac{\Gamma_{h\to f}}{\Gamma^{\rm SM}_{h\to f}} = \cos^2\alpha \quad (f \in ({\rm others\ in\ SM})) \quad \to \quad \frac{\Gamma_{h\to {\rm SM\,others}}}{\Gamma^{\rm SM}_{h\to {\rm SM\,others}}} = \cos^2\alpha, \tag{IV.6}$$

$$\frac{\Gamma_{h\to\gamma\gamma}}{\Gamma^{\rm SM}_{h\to\gamma\gamma}} = \left|\cos\alpha + \frac{1}{2}\frac{v^2}{m^2_{k^{\pm\pm}}} Q_k^2 C_{hkk} \frac{A_0^{\gamma\gamma}(\tau_k)}{A_1^{\gamma\gamma}(\tau_W) + N_C Q_t^2 A_{1/2}^{\gamma\gamma}(\tau_t)}\right|^2, \tag{IV.7}$$

$$\frac{\Gamma_{h\to Z\gamma}}{\Gamma^{\rm SM}_{h\to Z\gamma}} = \left|\cos\alpha - \frac{v^2}{m^2_{k^{\pm\pm}}} (2Q_k g_{Zkk})\, C_{hkk} \frac{A_0^{Z\gamma}(\tau_k,\lambda_k)}{v A_{\rm SM}^{Z\gamma}}\right|^2, \tag{IV.8}$$

with effective couplings

$$C_{hkk} = \cos\alpha\lambda_{\Phi k} - \sin\alpha\left(\frac{v'}{v}\right)\lambda_{\Sigma k}, \quad g_{Zkk} = -Q_k\left(\frac{s_W}{c_W}\right) \tag{IV.9}$$

and the form factor

$$A_{\rm SM}^{Z\gamma} = \frac{2}{v}\left[\cot\theta_W A_1^{Z\gamma}(\tau_W,\lambda_W) + N_C\frac{(2Q_t)(T_3^{(t)} - 2Q_t s_W^2)}{s_W c_W} A_{1/2}^{Z\gamma}(\tau_t,\lambda_t)\right]. \tag{IV.10}$$

$N_C\,(=3)$, $Q_t\,(=2/3)$, $Q_k\,(=2)$, $T_3^{(t)}\,(=1/2)$, c_W and s_W are the QCD color factor for quarks, the electric charges of the top quark, the doubly charged scalar in unit of the positron's one, the weak isospin of the top quark, and the cosine and the sine of the Weinberg angle θ_W,

respectively. The loop factors take the following forms,

$$A_1^{\gamma\gamma}(x) = -x^2\left[2x^{-2} + 3x^{-1} + 3(2x^{-1}-1)f(x^{-1})\right], \tag{IV.11}$$

$$A_{1/2}^{\gamma\gamma}(x) = 2x^2\left[x^{-1} + (x^{-1}-1)f(x^{-1})\right], \tag{IV.12}$$

$$A_0^{\gamma\gamma}(x) = -x^2\left[x^{-1} - f(x^{-1})\right], \tag{IV.13}$$

$$A_1^{Z\gamma}(x,y) = 4(3-\tan^2\theta_W)I_2(x,y) + \left[(1+2x^{-1})\tan^2\theta_W - (5+2x^{-1})\right]I_1(x,y), \tag{IV.14}$$

$$A_{1/2}^{Z\gamma}(x,y) = I_1(x,y) - I_2(x,y), \tag{IV.15}$$

$$A_0^{Z\gamma}(x,y) = I_1(x,y), \tag{IV.16}$$

with the functions

$$I_1(x,y) = \frac{xy}{2(x-y)} + \frac{x^2y^2}{2(x-y)^2}\left[f(x^{-1}) - f(y^{-1})\right] + \frac{x^2y}{(x-y)^2}\left[g(x^{-1}) - g(y^{-1})\right], \tag{IV.17}$$

$$I_2(x,y) = -\frac{xy}{2(x-y)}\left[f(x^{-1}) - f(y^{-1})\right]. \tag{IV.18}$$

In the above formulas, forms of the input variables to the loop factors τ_i and λ_i are defined as fractions by the Higgs boson mass (m_h) or the Z boson mass (m_Z)

$$\tau_i = \frac{4m_i^2}{m_h^2}, \quad \lambda_i = \frac{4m_i^2}{m_Z^2} \quad (i = t, W, k). \tag{IV.19}$$

The two ratios usually take values above one ($m_h \leq 2m_i$, $m_Z \leq 2m_i$). The two functions $f(z)$ and $g(z)$ ($z \equiv x^{-1}$ or y^{-1}) are formulated as

$$f(z) = \begin{cases} \arcsin^2\sqrt{z} & \text{for } z \leq 1, \\ -\frac{1}{4}\left[\log\left(\frac{1+\sqrt{1-z^{-1}}}{1-\sqrt{1-z^{-1}}}\right) - i\pi\right]^2 & \text{for } z > 1, \end{cases} \tag{IV.20}$$

$$g(z) = \begin{cases} \sqrt{z^{-1}-1}\arcsin\sqrt{z} & \text{for } z \leq 1, \\ \frac{\sqrt{1-z^{-1}}}{2}\left[\log\left(\frac{1+\sqrt{1-z^{-1}}}{1-\sqrt{1-z^{-1}}}\right) - i\pi\right] & \text{for } z > 1, \end{cases} \tag{IV.21}$$

where the situation $m_h \leq 2m_i$, $m_Z \leq 2m_i$ corresponds to $z \leq 1$.

To estimating the consistent parameter region with the latest results of the Higgs search at the LHC, we define the χ^2 valuable by use of the signal strength in Eq. (IV.1) as follows:

$$\chi^2 = \sum_{\substack{f=\gamma\gamma, ZZ^*, WW^*, \\ b\bar{b}, \tau\bar{\tau}\,(\text{ATLAS})}} \left(\frac{\mu_f - \hat{\mu}_f}{\hat{\sigma}_f}\right)^2 + \sum_{\substack{f=\gamma\gamma, ZZ^*, WW^*, \\ b\bar{b}, \tau\bar{\tau}\,(\text{CMS})}} \left(\frac{\mu_f - \hat{\mu}_f}{\hat{\sigma}_f}\right)^2. \tag{IV.22}$$

Here, we take the results of the five Higgs decay channels reported by the ATLAS and the CMS experiments into consideration, which are $h \to \gamma\gamma, h \to ZZ^* \to 4\ell, h \to WW^* \to$

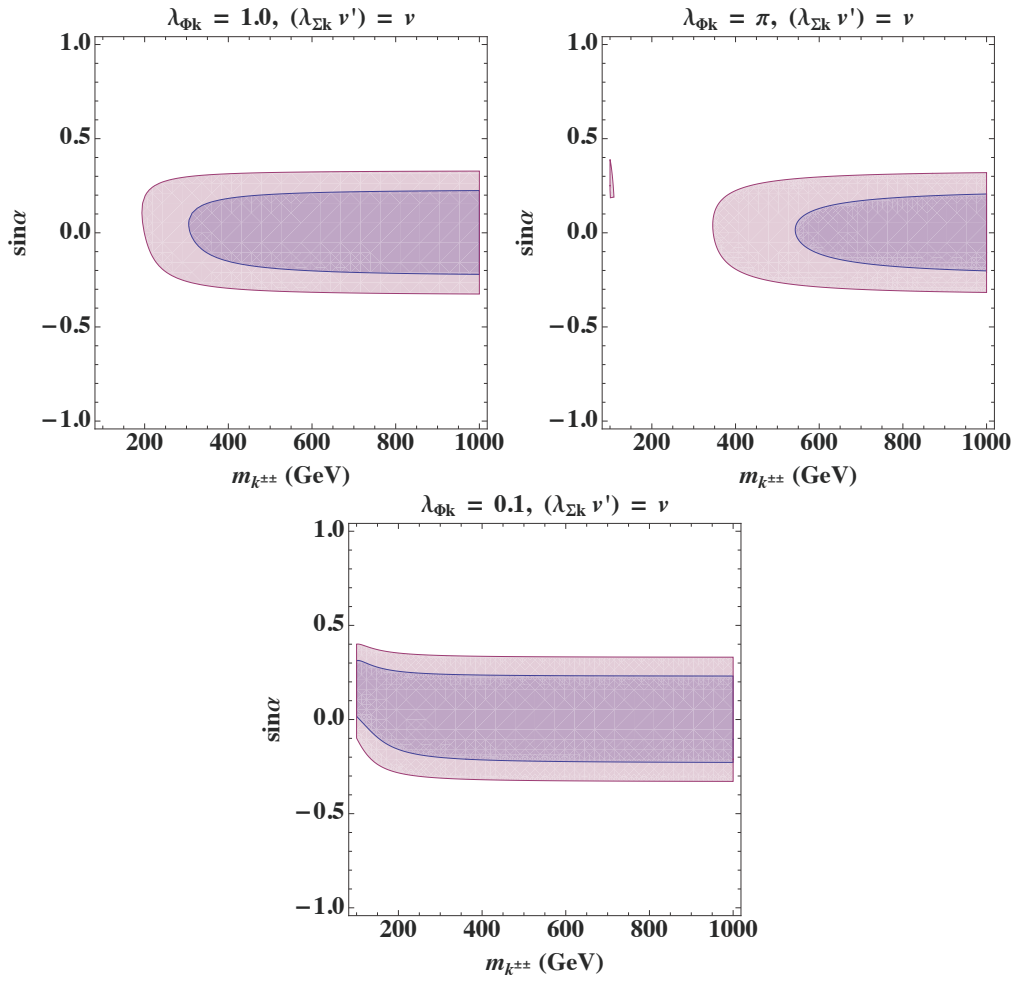

FIG. 4: The 1σ (blue) and 2σ (red) allowed regions of the global analysis based on the LHC data summarized in Table VI. From top left to bottom, we choose the parameters $(\lambda_{\Phi k}, \lambda_{\Sigma k} v') = (1.0, v)$, (π, v), $(0.1, v)$, respectively.

$\ell\nu\ell\nu, h \to b\bar{b}, h \to \tau\bar{\tau}$ summarized in Table VI. The two hatted symbols $\hat{\mu}_f$ and $\hat{\sigma}_f$ represent the corresponding central value and error, respectively. We assumed that each of ten experimental inputs follows the Gaussian distribution and there are no correlations among them. Also, when an error is asymmetric, we adopt its simple average as an input value of the corresponding $\hat{\sigma}_f$ for analysis. These simplifications are justified for our purpose of roughly estimating survived regions of the parameter space of this model.

In the following analysis, for simplicity, we focus on a reasonable situation in which the mass of the DM is around $m_h/2$ where the Higgs invisible channel to a pair of the DMs is near the threshold and negligible. Detailed discussions on the DM candidate are given

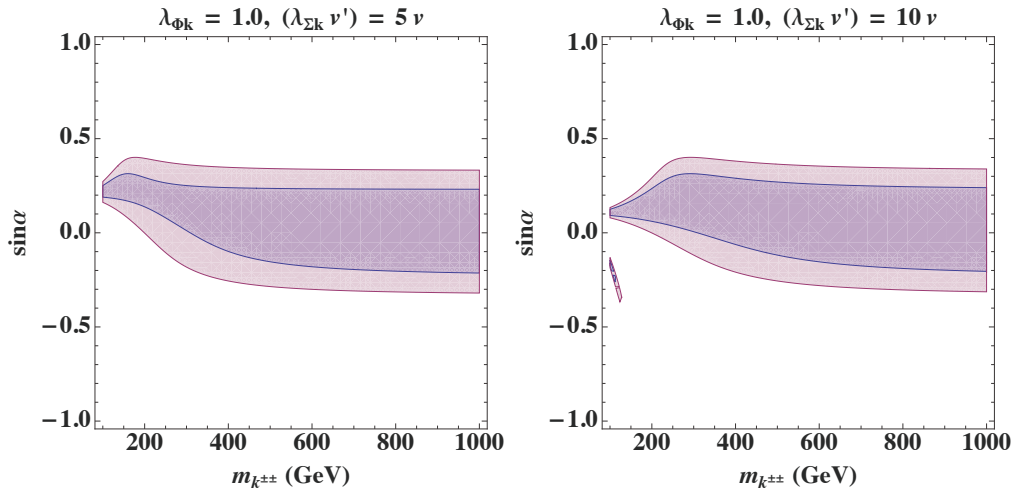

FIG. 5: The 1σ (blue) and 2σ (red) allowed regions of the global analysis based on the LHC data summarized in Table VI. From left to right, we choose the parameters $(\lambda_{\Phi k}, \lambda_{\Sigma k} v') = (1.0, 5v)$, $(1.0, 10v)$, respectively.

in Sec. V. Now, apparently, we see the five parameters $m_{k^{\pm\pm}}$, $\lambda_{\Phi k}$, $\lambda_{\Sigma k}$, v' and α govern the signal strengths of the Higgs boson. But in fact, as shown in Eq. (IV.9), $\lambda_{\Sigma k}$ and v' contribute to the Higgs physics only as the combination of $\lambda_{\Sigma k} v'$. Thus, four independent degrees of freedom are relevant in total.

We fix the two parameters $\lambda_{\Phi k}$ and $\lambda_{\Sigma k} v'$ in each of the following global fits for simplicity. Here, we consider the five possibilities, $(\lambda_{\Phi k}, \lambda_{\Sigma k} v') = (1.0, v)$, (π, v), $(0.1, v)$, $(1.0, 5v)$ and $(1.0, 10v)$ and search for their global minima on the remaining two variables $(m_{k^{\pm\pm}}, \sin\alpha)$ at first. The positions of each corresponding minimum are $(m_{k^{\pm\pm}}, \sin\alpha) = (74.7\,\mathrm{GeV}, -0.0759)$, $(109\,\mathrm{GeV}, -0.0774)$, $(65.0\,\mathrm{GeV}, 0.102)$, $(80.3\,\mathrm{GeV}, -0.0768)$ and $(87.5\,\mathrm{GeV}, -0.0804)$ with $\chi^2_{\mathrm{min}} \simeq 5.08$ (commonly in all the cases), respectively. The 1σ and 2σ boundaries are defined as the positions with $\chi^2 = \chi^2_{\mathrm{min}} + \Delta\chi^2_{1\sigma,2\sigma}$, where the values of $\Delta\chi^2_{1\sigma,2\sigma}$ are calculated by the cumulative distribution function of the χ^2-distribution with two degrees of freedom as $\Delta\chi^2_{1\sigma} = 2.296$, $\Delta\chi^2_{2\sigma} = 6.180$. The results are shown in Figs. 4–5. Small disconnected regions are found possibly due to accidental cancellations when $(\lambda_{\Phi k}, \lambda_{\Sigma k} v') = (\pi, v)$ in Fig. 4 and $(\lambda_{\Phi k}, \lambda_{\Sigma k} v') = (1.0, 10v)$ in Fig. 5. When we consider the doubly charged scalars with $m_{k^{\pm\pm}} = 500\,\mathrm{GeV}$, the range of α

$$|\sin\alpha| \lesssim 0.3 \tag{IV.23}$$

is roughly allowed within 2σ confidence levels, where actual upper bounds depend on contents of the two prefixed parameters.

V. ISSUES ON N_{R_1} DARK MATTER

In this section, we have discussions on dark matter related issues of this model. After the breakdown of the new global $U(1)$ symmetry, an accidental Z_2 symmetry still remains, which ensures the existence of a dark matter candidate. Under the assignment of the $U(1)$ charge in Table I, $N_{R_i}\,(i = 1, 2, 3)$ and $h_2^\pm$ hold negative parities, where the lightest one among them gets to be absolutely stable. After considering the aptness discussed in Sec. III B that $h_2^\pm$ (and also $h_1^\pm$) should be sufficiently heavy at around a few TeV to evade the constraints, *e.g.*, via the processes with LFV, the lightest right-hand neutrino, namely N_{R_1}, in our setup is usually stabilized by the symmetry and plays a significant role as dark matter.

An important point of our dark sector is in the mechanism for generating Majorana mass terms of N_R that originates from the spontaneous global $U(1)$ breaking accompanying a nonzero VEV of the field Σ_0. Through the mixing between Σ_0 and the Higgs doublet Φ, N_{R_1} can communicate with the SM particles, where the two neutral scalars h and H work as mediators. Here, we expect that a suitable amount of dark matter relics are left in the Universe through resonant effects via the h or H pole, where the mass of N_{R_1} is fixed around $m_h/2$ or $m_H/2$, respectively.

The relic abundance and the spin-independent cross section for direct detection of the candidate N_{R_1} are calculable by following a standard method. In the following part, we use the shorthand notation χ for showing the DM N_{R_1} (in the mass eigenstate as a Majorana fermion). Within the freeze-out approximation, the present-day relic density is evaluated as [119]

$$\Omega_\chi h^2 \simeq \frac{1.07 \times 10^9\,\mathrm{GeV}^{-1}}{\sqrt{g_*(x_f)}M_{\mathrm{Pl}}J(x_f)}, \tag{V.1}$$

where Ω_χ, $h\,(\simeq 0.7)$, M_{Pl} and g_* express the present-day energy density of χ, the present-day scaled Hubble parameter, the Planck mass and the number of the relativistic degrees of freedom, respectively. Note that the latest value of $\Omega_\chi h^2$ reported by the Planck experiment is $0.1196 \pm 0.0031\,(68\%\,\mathrm{C.L.})$ [120]. The valuable x_f is defined by the dark matter mass m_χ and the temperature at the freeze-out T_f as m_χ/T_f. The efficiency of the annihilation after

the freeze-out is described through the integral J:

$$J(x_f) = \int_{x_f}^{\infty} dx \frac{\langle \sigma v_{\rm rel} \rangle}{x^2}, \tag{V.2}$$

where $\langle \sigma v_{\rm rel} \rangle$ stands for the thermally averaged annihilation cross section multiplied with the relativistic relative velocity $v_{\rm rel}$. In this work, we adopt the sophisticated way for taking thermal average relativistically discussed in Refs. [121, 122], where $\langle \sigma v_{\rm rel} \rangle$ is estimated as

$$\langle \sigma v_{\rm rel} \rangle = \frac{\int_{4m_\chi^2}^{\infty} ds \frac{\sqrt{s-4m_\chi^2}}{16} W_{\chi\chi} K_1\left(\frac{\sqrt{s}}{T}\right)}{m_\chi^4 T \left[K_2\left(\frac{m_\chi}{T}\right)\right]^2} = \frac{\int_{4m_\chi^2}^{\infty} ds \sqrt{s-4m_\chi^2} W_{\chi\chi} K_1\left(\frac{\sqrt{s}}{m_\chi} x\right)}{16 m_\chi^5 x^{-1} \left[K_2(x)\right]^2}, \tag{V.3}$$

where x is defined as m_χ/T (like x_f) at the temperature T, $K_{1,2}$ are the modified Bessel functions of the second kind of order 1 and 2, respectively, and $W_{\chi\chi}$ is a Lorentz invariant variable describing the cross section multiplied with the Lorentz invariant flux factor $4E_\chi^2 v_{\rm rel}$. $W_{\chi\chi}$ is formulated in the center of mass system with the integration over the solid angle as

$$W_{\chi\chi} = \sum_f \frac{1}{32\pi^2} \sqrt{1 - \frac{4m_f^2}{s}} \int d\Omega \left| \overline{\mathcal{M}}(\chi\bar{\chi} \to f\bar{f}) \right|^2 \tag{V.4}$$

where we sum over all possible two-body final states consisting of the same particle f. The detail of the amplitudes is found in Appendix C. In the following numerical calculation, we simply use the fixed reasonable values $x_f = 20$ and $g_*(x_f) = 100$ throughout the calculations for brevity.

Our evaluation of the χ-nucleon spin-independent cross section is based on the discussions in Refs. [123, 124]. We consider the following effective Lagrangian for calculating the cross section at the leading order,

$$\mathcal{L}_{\rm eff} = \sum_{q=u,d,s} f_q m_q \bar{\chi}\chi\bar{q}q - \frac{\alpha_s}{4\pi} f_G \bar{\chi}\chi G^a_{\mu\nu} G^{a\mu\nu}, \tag{V.5}$$

where q, m_q, α_s, and $G^a_{\mu\nu}$ represent the corresponding quark fields, the quark masses, the QCD coupling strength, and the field strength of the gluon, respectively. The coefficients f_q (f_G) determine the effective interactions between the quarks (gluon) and the DM χ. The corresponding values in our model are

$$f_q = f_G = \frac{1}{2}\left(\frac{m_\chi}{vv'}\right)\left(-\frac{1}{m_h^2} + \frac{1}{m_H^2}\right)\cos\alpha \sin\alpha. \tag{V.6}$$

The spin-independent cross section with the target nucleus T is formulated by use of the spin-independent coupling of χ with nucleon f_N $(N = p, n)$ as

$$\sigma_{\rm SI}^T = \frac{4}{\pi}\mu_{T\chi}^2 \left| n_p f_p + n_n f_n \right|^2 , \tag{V.7}$$

where $\mu_{T\chi}$ is the reduced mass among the nucleus and the dark matter is defined as $\mu_{T\chi} \equiv m_T m_\chi/(m_T + m_\chi)$. m_T shows the mass of the target nucleus T, which contains n_p and n_n numbers of protons (p) and neutrons (n), respectively. The effective χ-nucleon (N) coupling f_N can be written down by the coefficients of the effective operators in $\mathcal{L}_{\rm eff}$ (f_q, f_G) and matrix elements (f_{Nq}, f_{NG}) as

$$f_N/m_N = \sum_{q=u,d,s} f_q f_{Nq} + \frac{2}{9} f_G f_{NG}, \tag{V.8}$$

with the concrete forms of the matrix elements,

$$\langle N| \, m_q \bar{q} q \, |N\rangle = f_{Nq} m_N, \quad 1 - \sum_{q=u,d,s} f_{Nq} = f_{NG}, \tag{V.9}$$

where the value of f_{NG} is calculable through the latter relation by the use of f_{Nq}. Like in Ref. [124], we adopt the following default values in the program `micrOMEGAs` [125]: $f_{nu} = 0.0110$, $f_{nd} = 0.0273$, $f_{ns} = 0.0447$.

The latest bound on the spin-independent scattering process was reported by the LUX experiment as an upper limit on the spin-independent (elastic) DM-nucleon cross section, which is approximately $10^{-45}\,{\rm cm}^2$ (when $m_\chi \sim 10^2\,{\rm GeV}$) with the 90% confidence level [126]. Here, we choose the neutron as the nucleon for putting a bound on our parameter space via the LUX result. Now, the (spin-independent) χ-neutron cross section is calculated with ease as

$$\begin{aligned}
\sigma_{\rm SI}^{N=n} &= \frac{4}{\pi}\mu_{n\chi}^2 \left| m_n \left(\sum_{q=u,d,s} f_{nq} + \frac{2}{9} f_{nG} \right) f_q \right|^2 \\
&= \frac{1}{\pi}\mu_{n\chi}^2 m_n^2 \, C^2 \left(\frac{m_\chi \cos\alpha \sin\alpha}{v v'} \right)^2 \left(-\frac{1}{m_h^2} + \frac{1}{m_H^2} \right)^2 ,
\end{aligned} \tag{V.10}$$

with

$$C = \frac{2}{9} + \frac{7}{9} \sum_{q=u,d,s} f_{nq} \simeq 0.287, \tag{V.11}$$

where similar calculations were done, *e.g.*, in Refs. [127, 128].

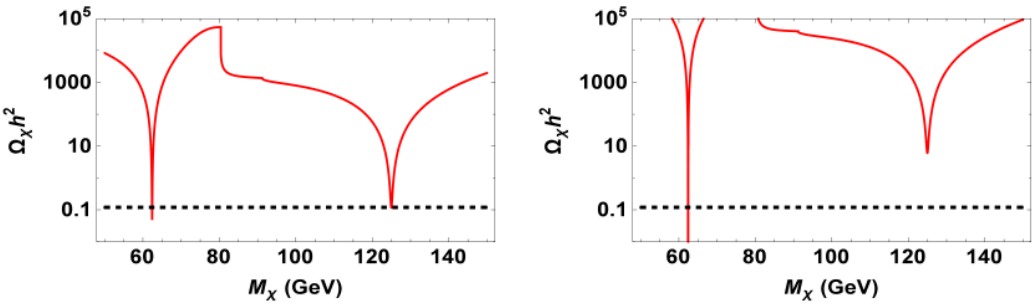

FIG. 6: Realized present-day relic densities of the dark matter candidate χ are shown as functions of m_χ. The other effective parameters are fixed as $\sin\alpha = 0.4$, $v' = 800\,\text{GeV}$, $m_H = 250\,\text{GeV}$, $m_{k^{\pm\pm}} = 500\,\text{GeV}$ (left panel) and $\sin\alpha = 0.5$, $v' = 5\,\text{TeV}$, $m_H = 250\,\text{GeV}$, $m_{k^{\pm\pm}} = 500\,\text{GeV}$ (right panel) for demonstration purposes, respectively. The area inside the two horizontal dashed lines (where the splitting is almost invisible) suggests the 2σ consistent region with the Planck data [$0.1196 \pm 0.0031\,(68\%\,\text{C.L.})$ [120]]. In the current setup, the relic density sharply drops around the two resonant regions around $m_h/2 \simeq 62.5\,\text{GeV}$ and $m_H/2 \simeq 125\,\text{GeV}$, where in the latter case, shown in the right panel, dropping is not sufficient for obtaining a proper amount of dark matter even around $m_H/2$ at present. We neglect the three- and four-body final states via virtual W and Z boson decays, which gives sizable modifications near the thresholds for producing gauge boson pairs [129, 130], since our interest is only around $m_h/2$ and $m_H/2$ where this correction is expected to be insignificant.

In the following calculation, we treat the variables α, m_H, and v' independently, which determines the coefficients $\lambda_{\Phi\Sigma}$, λ_Φ, and λ_Σ through the relations in Eqs. (II.6)–(II.7) as

$$\begin{aligned}
\lambda_{\Phi\Sigma} &= \frac{\sin\alpha\cos\alpha\,(m_H^2 - m_h^2)}{vv'}, \\
\lambda_\Phi &= \frac{\cos^2\alpha\, m_h^2 + \sin^2\alpha\, m_H^2}{2v^2}, \\
\lambda_\Sigma &= \frac{\sin^2\alpha\, m_h^2 + \cos^2\alpha\, m_H^2}{2v'^2}.
\end{aligned} \tag{V.12}$$

We set two quartic couplings $\lambda_{\Phi k}$ and $\lambda_{\Sigma k}$ as 1.0 and 0.1. In our scenario, v' tends to be $\mathcal{O}(1)\,\text{TeV}$ leading to suppression of the thermally averaged cross section describing pair annihilation processes; see Appendix C for detail forms. It would require a mechanism for enhancing the cross section. Hence, in this manuscript, we focus on the two resonant regions of m_χ around $m_h/2$ or $m_H/2$. Our requirement for the amount of the relics is that it should be within the $\pm 2\sigma$ range of the latest value reported by the Planck experiment

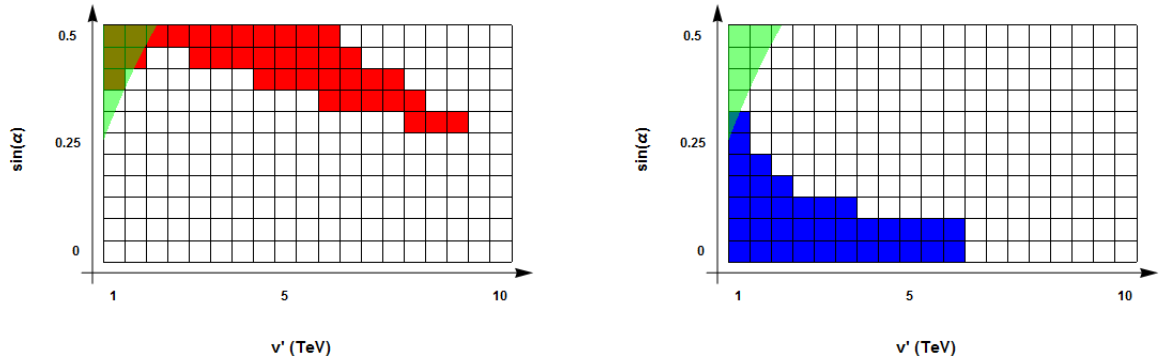

FIG. 7: The matrix plots indicate suitable choices of the two parameters v' and $\sin\alpha$ when we consider the situation of $m_H = 250\,\mathrm{GeV}$, $m_{k^{\pm\pm}} = 250\,\mathrm{GeV}$. We obtain the observed relic density in the red (blue) region in the left (right) panel when m_χ is around $m_h/2 \simeq 62.5\,\mathrm{GeV}$ ($m_H/2 \simeq 125\,\mathrm{GeV}$), respectively. The green region is excluded via excess of the invisible decay channel of the observed Higgs boson. No excluded region is found by the direct detection in the shown parameter range.

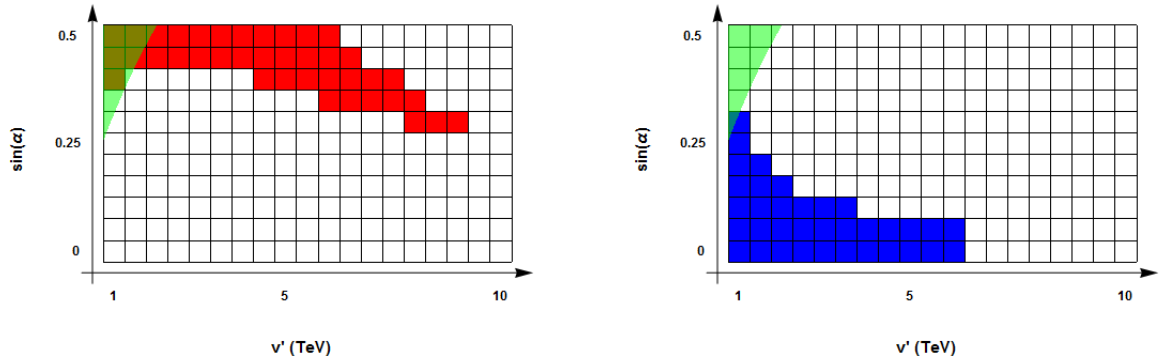

FIG. 8: The matrix plots for showing the region where a proper amount of the relic density is realized when $m_H = 250\,\mathrm{GeV}$, $m_{k^{\pm\pm}} = 500\,\mathrm{GeV}$. Conventions are the same with ones in Fig. 7. No excluded region is found by the direct detection in the shown parameter range.

$[0.1196 \pm 0.0031\,(68\%\,\mathrm{C.L.})\,[120]]$. In the following matrix plots, the values of v' and $\sin\alpha$ at the center of a square represent the inputs in the whole region shown by the square.

An important point is that all the effective diagrams of this pair annihilation of χ are Higgs

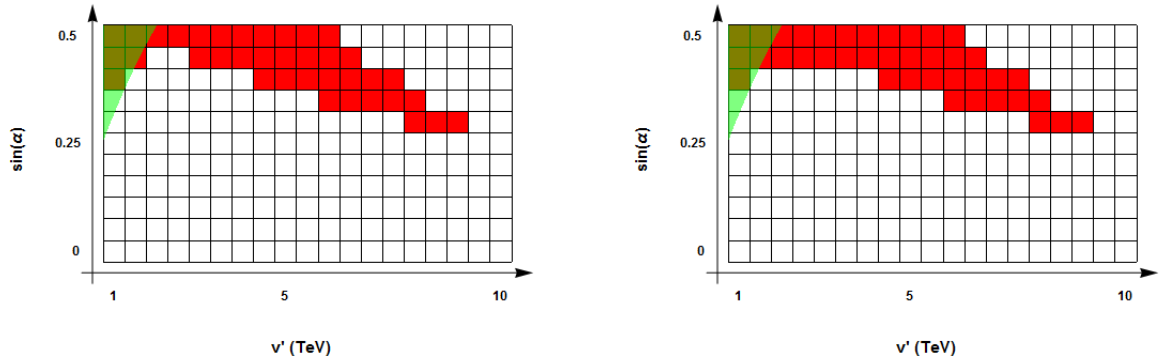

FIG. 9: Similar plots as Figs. 7 and 8 when $m_H = 500\,\mathrm{GeV}$, $m_{k^{\pm\pm}} = 250\,\mathrm{GeV}$ (left) and $m_H = 500\,\mathrm{GeV}$, $m_{k^{\pm\pm}} = 500\,\mathrm{GeV}$ (right), respectively. Here, no solution is found around $m_\chi \simeq m_H/2 \simeq 250\,\mathrm{GeV}$, while one around $m_\chi \simeq m_h/2 \simeq 62.5\,\mathrm{GeV}$ is still there. The green region is excluded by the invisible decay of the 125 GeV Higgs. No excluded region is found by the direct detection in the shown parameter range.

mediated.[8] Like the couplings between the observed fermions and the 125 GeV Higgs boson in the SM, the DM-portal scalar couplings are proportional to the factor m_χ/v'. In Fig. 6, we present realized present-day relic densities of the dark matter candidate χ as functions of m_χ, where the other effective parameters are fixed as $\sin\alpha = 0.4$, $v' = 800\,\mathrm{GeV}$, $m_H = 250\,\mathrm{GeV}$, $m_{k^{\pm\pm}} = 500\,\mathrm{GeV}$ (left panel) and $\sin\alpha = 0.5$, $v' = 5\,\mathrm{TeV}$, $m_H = 250\,\mathrm{GeV}$, $m_{k^{\pm\pm}} = 500\,\mathrm{GeV}$ (right panel), respectively. Here, we can see that a suppression due to a huge v' in the latter case and the point around the heavier resonance of H is not suitable for a correct amount of DM today. Around the lighter one of h, less s-channel propagator suppression could be expected and thus the solution around this pole still remains.

Another critical variable in the relic calculation is the mixing angle α among the two CP even scalars h and H. If $\sin\alpha$ is close to zero, contributions from the mediator h are diminished significantly due to almost zeroness of the couplings between χ and the SM particles in the final state. Thereby, a suitable amount of the mixing is requested for the solution near $m_h/2$. In the following analysis, we focus on non-negative values in $\sin\alpha$

[8] Note that the processes $N_{R_1}\bar{N}_{R_1} \to \ell_i^+\ell_j^-\,(i,j=1,2,3)$ with exchanging $h_2^\pm$ in t-channel, which are important in similar situations [7, 131], are ineffective and neglected in the present scenario because the lower bound on $m_{h_2^\pm}$ is around a few TeV and decoupled as shown in subsection III B.

since the sign of $\sin\alpha$ is insignificant in the resonant regions.[9] Also, we ignore the range of $|\sin\alpha| > 0.5$ since no allowed region was found in the results of the global analyses shown in Figs. 4–5.

As actual examples, we investigate the four possibilities in $(m_H, m_{k^{\pm\pm}})$ of $(250\,\mathrm{GeV}, 250\,\mathrm{GeV})$ in Fig. 7; $(250\,\mathrm{GeV}, 500\,\mathrm{GeV})$ in Fig. 8; and $(500\,\mathrm{GeV}, 250\,\mathrm{GeV})$ and $(500\,\mathrm{GeV}, 500\,\mathrm{GeV})$ in Fig. 9, respectively. The regions covered with the color green are excluded, where the branching ratio of the observed Higgs boson to invisible pairs exceeds the 95% confidence level upper bound 0.29 reported by the ATLAS experiment [132].[10] The value of v' and α almost completely determines the profiles since the primary final state with invisibleness is a pair of the NG bosons G. We mention that no exclusion from the direct detection process is found in the shown parameter ranges since the elastic scattering cross section is suppressed by the large VEV v'. We observe small differences originating from the value of $m_{k^{\pm\pm}}$ since in the DM mass range of $m_\chi \lesssim m_{k^{\pm\pm}}$, $k^{\pm\pm}$ can contribute to the relic density only indirectly through the total widths Γ_h and Γ_H.[11]

A suggestive aspect via the results is that only around the $m_h/2$ is possible when m_H gets large as 500 GeV because the suppression via the heavy resonant particle could eliminate the solution near $m_H/2$. On the other hand, as discussed in Sec. IV, the 7 and 8 TeV LHC results restrict the scalar mixing angle α, where we quote a typical bound we obtained, $|\sin\alpha| \lesssim 0.3$. For making the DM solution around $m_h/2$ realizable, we should select the absolute value of the mixing angle $|\sin\alpha|$ around or more than 0.3 as shown in Figs. 7–9. Let us remind the reader that the sign of $\sin\alpha$ does not affect the result (calculated in $\sin\alpha \geq 0$) significantly. In addition, here, the value of v' is also constrained as around or less than 9 TeV in the case of $m_\chi \simeq m_h/2$. In conclusion, the present scenario is still viable, but a

[9] We mention details of this point. The sign of $\sin\alpha$ affects results only through the amplitude of $\chi\bar{\chi} \to hh$ and the partial decay width of $h/H \to \gamma\gamma$ and $h/H \to Z\gamma$ in the s-channel propagators. In the DM masses which we consider, the amplitude gives only a subleading contribution. The effect coming from the widths is also negligible since the branching ratios of $h/H \to \gamma\gamma$ and $h/H \to Z\gamma$ are pretty small.

[10] In this estimation, the Standard Model production cross section was assumed in $m_h = 125\,\mathrm{GeV}$. Here, we do not care about this point seriously and simply utilize this result for putting a bound on the present scenario.

[11] We simply ignore the process $\chi\chi \to k^{++}k^{--}$ in the case near the kinetic boundary, $m_H = 500\,\mathrm{GeV}$ and $m_{k^{\pm\pm}} = 250\,\mathrm{GeV}$, where the heavier resonant region corresponds to $m_\chi \simeq 250\,\mathrm{GeV}$. Here, we do not consider the lighter $k^{\pm\pm}$ with $100 \sim 250\,\mathrm{GeV}$ mass, the possibility of which was examined in the global fits in section IV.

part of the parameter space generating a suitable amount of relics comes to be on the edge. Note that our calculation would be applicable for a rather general setup of a fermion dark matter communicating the SM sector through two scalars with renormalizable interactions and $\mathcal{O}(1)$ TeV v' after the decoupling of $k^{\pm\pm}$.

VI. SUMMARY AND CONCLUSION

In this paper, we proposed a three loop radiative neutrino mass scenario with an *isolated* doubly charged singlet scalar $k^{\pm\pm}$ without couplings to the charged leptons at the leading order for solving an undesirable situation in our previous study [1]. The previous scenario has the same particle contents of charged singlet scalars with the present model, two singly charged ones ($h_1^\pm$, $h_2^\pm$) and one doubly charged one ($k^{\pm\pm}$), but assignments of additional global symmetries are different, which makes a difference in interactions associated with the charged bosons.

In the previous case without Majorana neutrinos, $k^{\pm\pm}$ should attach the charged leptons at the leading order to generate a neutrino mass matrix at the three loop level. But a side effect due to this type of couplings with LFV could be serious from a phenomenological point of view. Because of resultant tree-level contributions to LFV processes, related couplings are severely constrained, where realized neutrino masses get to be smaller than the observed values. Increasing scalar trilinear couplings with charged scalars appearing in the numerator of elements of the loop-induced neutrino mass matrix seems to be an option. However, the largeness in the trilinear couplings tends to destabilize the vacuum rapidly. Making all of the charged scalars very heavy is a solution since the scalar trilinear couplings do not contribute to LFV at the leading order and the ratio of the trilinear couplings divided by the masses of the charged scalars can remain "sizable" for the observed neutrino masses. Here, however, a typical mass scale of the charged bosons should be around 10 TeV, where we cannot expect a signal suggesting the existence of the particles at the LHC.

Our modified setup in the assignment of a global $U(1)$ symmetry brings us a better situation. Introducing Majorana neutrinos allows $k^{\pm\pm}$ to be away from the charged leptons. Now the LFV is relatively relaxed, and at least a part of the couplings contributing to the neutrino mass can take larger values. Thus, scalar trilinear couplings need not to be drastically large, and, as a result, vacuum destabilization is alleviated. We found that a

few hundred GeV $k^{\pm\pm}$ is realizable, which can be tested at the ongoing LHC experiment, even though the two singly charged scalars are still very heavy at around a few TeV. It is noteworthy that the associated NG boson G does not generate dangerous interactions that severely restrict the decay constant v'. The constant v' can takes a value around the TeV scale with no harm.

Another constraint on the system comes from the mixing of two CP even neutral scalars, which are mixed states between the component of the $SU(2)_L$ doublet Φ in the SM and the corresponding part of a complex $SU(2)_L$ singlet scalar Σ_0 for the spontaneous symmetry breaking of the global $U(1)$. After the breakdown, Majorana fermions obtain masses via the Higgs mechanism and a residual discrete parity ensures the stability of an accidental DM candidate of the lightest Majorana neutrino N_{R_1}. This mixing angle plays a very important role in the DM-related phenomena in this model since the candidate can couple to the SM sector only through the two mass eigenstates of the CP even scalars $h\,(= 125\,\mathrm{GeV})$ and H. Note that the two singly charged scalars should be decoupled in our scenario and diagrams associated with them are negligible.

The latest LHC result of the Higgs search by the ATLAS and the CMS experiments puts a stringent bound on the mixing angle α, $|\sin\alpha| \lesssim 0.3$ as a roughly estimated bound through a global analysis. A typical scale of the VEV of Σ_0 would be around a few TeV scale, where the DM pair annihilation cross section is significantly suppressed since the Yukawa couplings between N_{R_1} and Σ_0 are inversely proportional to the VEV. When the DM mass is around the two resonant regions, $m_h/2$ and $m_H/2$, the cross section is enhanced very much. But we found that when M_H is heavy at around $500\,\mathrm{GeV}$, the possibility near $m_H/2$ is closed due to the propagator suppression of the massive mediator. On the other hand, to activate the solution around $m_h/2$, the mixing angle α should be large to a certain degree to ensure a sizable interaction between the DM and SM particles. Typically, a required value in this direction is $|\sin\alpha| \gtrsim 0.3$, which would not have large overlaps with the preferred area obtained via the global analysis on the Higgs search results.

In spite of the insignificance of the bounds via the invisible $125\,\mathrm{GeV}$ Higgs decay and the DM direct detection because of the coupling suppression via the huge VEV of Σ_0, experimental data in Higgs physics put sizable constraints on our scenario. In the near future, updated Higgs results could declare validity of our scenario much more precisely. Also, searching for a suitable way to discriminate the present scenario from other models

with charged scalars will be an important task at the LHC and other future colliders.

Acknowledgments

K. N. is grateful for Tomohiro Abe, Motoi Endo, Masahiro Ibe, Shinya Kanemura, Tetsuo Shindou, Hiroaki Sugiyama, Koji Tsumura and Toshifumi Yamashita for kind suggestions and useful discussions. H. O. is sincerely grateful for all the KIAS members, Korean cordial persons, foods, culture, weather, and all the other things. This work is supported in part by NRF Research No. 2009-0083526 (Y. O.) of the Republic of Korea.

Appendix A: Analytic forms of loop functions for LFV

In this appendix, we show analytic forms of the loop functions for processes with LFV. The functions for $\ell \to \ell\gamma$ in Eq. (II.34) are obtained as

$$I'_{1,a} = \frac{1}{(4\pi)^2}\int_0^1 dx \int_0^{1-x} dy \; \frac{x(2x-1)}{(x+y)m^2_{h_2^\pm} + (1-x-y)M^2_{N_a}}$$
$$= \begin{cases} \frac{1}{(4\pi)^2} \frac{9m^4_{h_2^\pm}M^2_{N_a} + 9m^2_{h_2^\pm}M^4_{N_a}\left(2\log\left(\frac{M^2_{N_a}}{m^2_{h_2^\pm}}\right)+1\right) + M^6_{N_a}\left(6\log\left(\frac{M^2_{N_a}}{m^2_{h_2^\pm}}\right)-17\right) - m^6_{h_2^\pm}}{36\left(m^2_{h_2^\pm} - M^2_{N_a}\right)^4} & (\text{for } m_{h_2^\pm} \neq M_{N_a}), \\ 0 & (\text{for } m_{h_2^\pm} = M_{N_a}), \end{cases} \tag{A.1}$$

$$I'_{2,a} = \frac{1}{(4\pi)^2}\int_0^1 dx \int_0^{1-x} dy \; \frac{x(2y-1)}{(x+y)m^2_{h_2^\pm} + (1-x-y)M^2_{N_a}}$$
$$= \begin{cases} \frac{1}{(4\pi)^2} \frac{27m^4_{h_2^\pm}M^2_{N_a} - 9m^2_{h_2^\pm}M^4_{N_a}\left(2\log\left(\frac{m^2_{h_2^\pm}}{M^2_{N_a}}\right)+3\right) + M^6_{N_a}\left(6\log\left(\frac{m^2_{h_2^\pm}}{M^2_{N_a}}\right)+5\right) - 5m^6_{h_2^\pm}}{36\left(m^2_{h_2^\pm} - M^2_{N_a}\right)^4} & (\text{for } m_{h_2^\pm} \neq M_{N_a}), \\ -\frac{1}{(4\pi)^2}\frac{1}{12m^2_{h_2^\pm}} & (\text{for } m_{h_2^\pm} = M_{N_a}). \end{cases} \tag{A.2}$$

Note that when we take the limit $M_{N_a} \to 0$, $I'_{1,a}$ and $I'_{2,a}$ are reduced to $I_{1,a}$ and $I_{2,a}$ (up to the difference of $m_{h_1^\pm}$ and $m_{h_2^\pm}$), respectively,

$$I'_{1,a} \to -\frac{1}{(4\pi)^2}\frac{1}{36m^2_{h_2^\pm}}, \quad I'_{2,a} \to -\frac{1}{(4\pi)^2}\frac{5}{36m^2_{h_2^\pm}}. \tag{A.3}$$

The functions $J_{1,ab}$ and $J_{2,ab}$ for describing the $\ell \to 3\ell$ processes in Eq. (II.40) take the following forms

$$J_{1,ab} = \frac{1}{(4\pi)^2}\int_0^1 dx \int_0^{1-x} dy \; \frac{1-x-y}{\left[xM_{N_a}^2 + yM_{N_b}^2 + (1-x-y)m_{h_2^\pm}^2\right]}$$

$$= \frac{1}{(4\pi)^2}\left\{ \frac{m_{h_2^\pm}^6 M_{N_a}^2 + m_{h_2}^4 M_{N_a}^4 \left(\log\left(\frac{M_{N_a}^2}{m_{h_2^\pm}^2}\right)-1\right) - m_{h_2^\pm}^6 M_{N_b}^2 + m_{h_2^\pm}^2 M_{N_a}^4 M_{N_b}^2 \left(2\log\left(\frac{m_{h_2^\pm}^2}{M_{N_a}^2}\right)+1\right)}{2\left(M_{N_a}^2 - M_{N_b}^2\right)\left(m_{h_2^\pm}^2 - M_{N_a}^2\right)^2\left(m_{h_2^\pm}^2 - M_{N_b}^2\right)^2} \right.$$

$$\left. + \frac{m_{h_2^\pm}^4 M_{N_b}^4 \left(\log\left(\frac{m_{h_2^\pm}^2}{M_{N_b}^2}\right)+1\right) + m_{h_2^\pm}^2 M_{N_a}^2 M_{N_b}^4 \left(2\log\left(\frac{M_{N_b}^2}{m_{h_2^\pm}^2}\right)-1\right) + M_{N_a}^4 M_{N_b}^4 \log\left(\frac{M_{N_a}^2}{M_{N_b}^2}\right)}{2\left(M_{N_a}^2 - M_{N_b}^2\right)\left(m_{h_2^\pm}^2 - M_{N_a}^2\right)^2\left(m_{h_2^\pm}^2 - M_{N_b}^2\right)^2} \right\}$$

$$(\text{for } m_{h_2^\pm} \neq M_{N_a} \neq M_{N_b}), \quad \text{(A.4)}$$

$$J_{2,ab} = \frac{1}{(4\pi)^2}\int_0^1 dx \int_0^{1-x} dy \; \frac{1-x-y}{\left[xM_{N_a}^2 + yM_{N_b}^2 + (1-x-y)m_{h_2^\pm}^2\right]^2}$$

$$= \frac{m_{h_2^\pm}^4 \left(M_{N_a}^2 \left(\log\left(\frac{m_{h_2^\pm}^2}{M_{N_a}^2}\right)-1\right) + M_{N_b}^2 \left(\log\left(\frac{M_{N_b}^2}{m_{h_2^\pm}^2}\right)+1\right)\right) + m_{h_2^\pm}^2 \left(2M_{N_a}^2 M_{N_b}^2 \log\left(\frac{M_{N_a}^2}{M_{N_b}^2}\right) + M_{N_a}^4 - M_{N_b}^4\right) + M_{N_a}^2 M_{N_b}^4 \left(\log\left(\frac{m_{h_2^\pm}^2}{M_{N_a}^2}\right)+1\right) + M_{N_a}^4 M_{N_b}^2 \left(\log\left(\frac{M_{N_b}^2}{m_{h_2^\pm}^2}\right)-1\right)}{(4\pi)^2\left(m_{h_2^\pm}^2 - M_{N_a}^2\right)^2\left(m_{h_2^\pm}^2 - M_{N_b}^2\right)^2\left(M_{N_a}^2 - M_{N_b}^2\right)}$$

$$(\text{for } m_{h_2^\pm} \neq M_{N_a} \neq M_{N_b}), \quad \text{(A.5)}$$

where the following specific cases are also obtained:

$$J_{1,ab} \to \begin{cases} \frac{1}{(4\pi)^2} \frac{2m_{h_2^\pm}^2 M_{N_a}^2 \log\left(\frac{M_{N_a}^2}{m_{h_2^\pm}^2}\right) - M_{N_a}^4 + m_{h_2^\pm}^4}{2\left(m_{h_2^\pm}^2 - M_{N_a}^2\right)^3} & (\text{for } M_{N_a} = M_{N_b} \neq m_{h_2^\pm}), \\ \frac{1}{(4\pi)^2}\frac{1}{2m_{h_2^\pm}^2} & (\text{for } M_{N_a} = M_{N_b} = m_{h_2^\pm}), \end{cases} \quad \text{(A.6)}$$

$$J_{2,ab} \to \begin{cases} \frac{1}{(4\pi)^2} \frac{m_{h_2^\pm}^2 \left(\log\left(\frac{m_{h_2^\pm}^2}{M_{N_a}^2}\right)-2\right) + M_{N_a}^2 \left(\log\left(\frac{m_{h_2^\pm}^2}{M_{N_a}^2}\right)+2\right)}{\left(m_{h_2^\pm}^2 - M_{N_a}^2\right)^3} & (\text{for } M_{N_a} = M_{N_b} \neq m_{h_2^\pm}), \\ \frac{1}{(4\pi)^2}\frac{1}{6m_{h_2^\pm}^4} & (\text{for } M_{N_a} = M_{N_b} = m_{h_2^\pm}). \end{cases} \quad \text{(A.7)}$$

Appendix B: Partial widths of CP even scalars

In this appendix, we represent a part of partial decay widths with nontrivial forms of the two CP even scalars h and H with our notation for loop functions.

$$\Gamma_{h\to GG} = \frac{m_h^3}{32\pi v'^2}\sin^2\alpha, \tag{B.1}$$

$$\Gamma_{h\to N_{R_1}\bar{N}_{R_1}} = \frac{1}{16\pi}\left(\frac{M_{N_1}}{v'}\right)^2 m_h\left(1-\frac{4M_{N_1}^2}{m_h^2}\right)^{3/2}\sin^2\alpha, \tag{B.2}$$

$$\Gamma_{H\to GG} = \frac{m_H^3}{32\pi v'^2}\cos^2\alpha, \tag{B.3}$$

$$\Gamma_{H\to N_{R_1}\bar{N}_{R_1}} = \frac{1}{16\pi}\left(\frac{M_{N_1}}{v'}\right)^2 m_H\left(1-\frac{4M_{N_1}^2}{m_H^2}\right)^{3/2}\cos^2\alpha, \tag{B.4}$$

$$\Gamma_{H\to 2h} = \frac{1}{32\pi m_H}|C_{Hhh}|^2\sqrt{1-\frac{4m_h^2}{m_H^2}}, \tag{B.5}$$

$$\Gamma_{h\to gg} = \frac{G_F\alpha_s^2 m_h^3}{36\sqrt{2}\pi^3}\left|\frac{3}{4}\left(A_{1/2}^{\gamma\gamma}(\tau_t)\right)\cos\alpha\right|^2, \tag{B.6}$$

$$\Gamma_{h\to\gamma\gamma} = \frac{G_F\alpha_{\rm EM}^2 m_h^3}{128\sqrt{2}\pi^3}\left|\left(A_1^{\gamma\gamma}(\tau_W)+N_C Q_t^2 A_{1/2}^{\gamma\gamma}(\tau_t)\right)\cos\alpha+\frac{1}{2}\frac{v^2}{m_{k^{\pm\pm}}^2}Q_k^2 C_{hkk}A_0^{\gamma\gamma}(\tau_k)\right|^2, \tag{B.7}$$

$$\Gamma_{h\to Z\gamma} = \frac{\alpha_{\rm EM}^2 m_h^3}{512\pi^3}\left(1-\frac{m_Z^2}{m_h^2}\right)^3\left|A_{\rm SM}^{Z\gamma}\cos\alpha-\frac{v}{m_{k^{\pm\pm}}^2}\left(2Q_k g_{Zkk}\right)C_{hkk}A_0^{Z\gamma}(\tau_k,\lambda_k)\right|^2, \tag{B.8}$$

$$\Gamma_{H\to gg} = \frac{G_F\alpha_s^2 m_H^3}{36\sqrt{2}\pi^3}\left|\frac{3}{4}\left(A_{1/2}^{\gamma\gamma}(\tau_t')\right)\sin\alpha\right|^2, \tag{B.9}$$

$$\Gamma_{H\to\gamma\gamma} = \frac{G_F\alpha_{\rm EM}^2 m_H^3}{128\sqrt{2}\pi^3}\left|\left(A_1^{\gamma\gamma}(\tau_W')+N_C Q_t^2 A_{1/2}^{\gamma\gamma}(\tau_t')\right)\sin\alpha+\frac{1}{2}\frac{v^2}{m_{k^{\pm\pm}}^2}Q_k^2 C_{Hkk}A_0^{\gamma\gamma}(\tau_k')\right|^2, \tag{B.10}$$

$$\Gamma_{H\to Z\gamma} = \frac{\alpha_{\rm EM}^2 m_H^3}{512\pi^3}\left(1-\frac{m_Z^2}{m_H^2}\right)^3\left|A_{\rm SM}^{Z\gamma}(\tau_{W,t}\to\tau_{W,t}')\sin\alpha-\frac{v}{m_{k^{\pm\pm}}^2}\left(2Q_k g_{Zkk}\right)C_{Hkk}A_0^{Z\gamma}(\tau_k',\lambda_k)\right|^2, \tag{B.11}$$

with C_{hkk} in Eq. (IV.9) and the parameters

$$\tau_i' = \frac{4m_i^2}{m_H^2}\ (i=t,W,k), \quad C_{Hkk} = \sin\alpha\lambda_{\Phi k}+\cos\alpha\lambda_{\Sigma k}\left(\frac{v'}{v}\right). \tag{B.12}$$

G_F and α_s are the Fermi constant and the QCD coupling strength, respectively. Note that in the calculation $\Gamma_{H\to Z\gamma}$, the replacement $\tau_i\to\tau_i'$ in the factor $A_{\rm SM}^{Z\gamma}$ is required. One can refer to Sec. IV for the detail of loop functions.

Appendix C: Matrix elements for N_{R_1} dark matter annihilations

In this appendix, we summarize the averaged matrix elements squared for relic density calculation of the dark matter candidate N_{R_1} through pair annihilations. Note that no symmetric factor is included originating from identical final states in the following forms, which should be considered in the integration over the solid angle for estimating the thermal average of the cross section $\langle \sigma v_{\rm rel} \rangle$.

$$|\overline{\mathcal{M}}(N_{R_1}\bar{N}_{R_1} \to f\bar{f})|^2 = 4N_{C_f}\left(\frac{M_{N_1} m_f s_\alpha c_\alpha}{vv'}\right)^2 \left|\frac{1}{s-m_h^2+im_h\Gamma_h} - \frac{1}{s-m_H^2+im_H\Gamma_H}\right|^2 \times \left[(p_1\cdot p_2) - M_{N_1}^2\right]\left[(k_1\cdot k_2) - m_f^2\right], \tag{C.1}$$

$$|\overline{\mathcal{M}}(N_{R_1}\bar{N}_{R_1} \to ZZ)|^2 = \left(\frac{M_{N_1} g_2 M_W s_\alpha c_\alpha}{v' c_W^2}\right)^2 \left|\frac{1}{s-m_h^2+im_h\Gamma_h} - \frac{1}{s-m_H^2+im_H\Gamma_H}\right|^2 \times \left[(p_1\cdot p_2) - M_{N_1}^2\right]\left[2 + \frac{(k_1\cdot k_2)^2}{M_Z^4}\right], \tag{C.2}$$

$$|\overline{\mathcal{M}}(N_{R_1}\bar{N}_{R_1} \to W^+W^-)|^2 = \left(\frac{M_{N_1} g_2 M_W s_\alpha c_\alpha}{v'}\right)^2 \left|\frac{1}{s-m_h^2+im_h\Gamma_h} - \frac{1}{s-m_H^2+im_H\Gamma_H}\right|^2 \times \left[(p_1\cdot p_2) - M_{N_1}^2\right]\left[2 + \frac{(k_1\cdot k_2)^2}{M_W^4}\right], \tag{C.3}$$

$$|\overline{\mathcal{M}}(N_{R_1}\bar{N}_{R_1} \to GG)|^2 = 4\left(\frac{M_{N_1}}{vv'}\right)^2 (k_1\cdot k_2)^2 \left|\frac{s_\alpha^2}{s-m_h^2+im_h\Gamma_h} + \frac{c_\alpha^2}{s-m_H^2+im_H\Gamma_H}\right|^2 \times \left[(p_1\cdot p_2) - M_{N_1}^2\right], \tag{C.4}$$

$$|\overline{\mathcal{M}}(N_{R_1}\bar{N}_{R_1} \to hh)|^2 = \left(\frac{M_{N_1}}{v'}\right)^2 \left|\frac{s_\alpha C_{hhh}}{s-m_h^2+im_h\Gamma_h} - \frac{c_\alpha C_{Hhh}}{s-m_H^2+im_H\Gamma_H}\right|^2 \times \left[(p_1\cdot p_2) - M_{N_1}^2\right], \tag{C.5}$$

where N_{C_f} shows the color factor 3 (1) when f is a quark (lepton), p_1, p_2 and k_1, k_2 are initial- and final-state momenta, respectively. s is defined as $s = (p_1+p_2)^2 = (k_1+k_2)^2$. Here, we use the shorthand notations of $c_\alpha \equiv \cos\alpha$ and $s_\alpha \equiv \sin\alpha$. The forms of effective couplings describing scalar self interactions are

$$C_{hhh} = 3\lambda_{\Phi\Sigma}\left(v(s_\alpha^2 c_\alpha) - v'(c_\alpha^2 s_\alpha)\right) + 6\lambda_\Phi v c_\alpha^3 - 6\lambda_\Sigma v' s_\alpha^3, \tag{C.6}$$

$$C_{Hhh} = \lambda_{\Phi\Sigma}\left(v\left(s_\alpha^3 - 2c_\alpha^2 s_\alpha\right) + v'\left(c_\alpha^3 - 2c_\alpha s_\alpha^2\right)\right) + 6\lambda_\Phi v c_\alpha^2 s_\alpha + 6\lambda_\Sigma v' s_\alpha^2 c_\alpha. \tag{C.7}$$

We mention that the processes $N_{R_1}\bar{N}_{R_1}$ into HH, hH, $k^{++}k^{--}$, $h_1^+h_1^-$ and $h_2^+h_2^-$ are ineffective in our discussion when the mass of the DM is around $m_h/2$ or $m_H/2$ considering the bounds discussed in Sec. III–IV.

Note that the processes $N_{R_1}\bar{N}_{R_1} \to \ell_i^+ \ell_j^-$ $(i,j=1,2,3)$ with the exchange of $h_2^\pm$ in the t channel, which are important in similar situations [7, 131], are ineffective and neglected in the present scenario because the lower bound on $m_{h_2^\pm}$ is around a few TeV and decoupled as shown in Sec. III B. We neglect the three- and four-body final states via virtual W and Z boson decays, which gives sizable modifications near the thresholds for producing gauge boson pairs [129, 130], since our interest is only around $m_h/2$ and $m_H/2$ where this correction is expected to be ineffective.

[1] H. Hatanaka, K. Nishiwaki, H. Okada and Y. Orikasa, Nucl. Phys. B **894**, 268 (2015) [arXiv:1412.8664 [hep-ph]].

[2] G. Aad *et al.* [ATLAS Collaboration], Phys. Lett. B **716**, 1 (2012) [arXiv:1207.7214 [hep-ex]].

[3] S. Chatrchyan *et al.* [CMS Collaboration], Phys. Lett. B **716**, 30 (2012) [arXiv:1207.7235 [hep-ex]].

[4] A. Zee, Phys. Lett. B **93**, 389 (1980) [Erratum-ibid. B **95**, 461 (1980)].

[5] T. P. Cheng and L. F. Li, Phys. Rev. D **22**, 2860 (1980).

[6] A. Zee, Nucl. Phys. B **264**, 99 (1986); K. S. Babu, Phys. Lett. B **203**, 132 (1988).

[7] L. M. Krauss, S. Nasri and M. Trodden, Phys. Rev. D **67**, 085002 (2003) [arXiv:hep-ph/0210389].

[8] E. Ma, Phys. Rev. D **73**, 077301 (2006) [hep-ph/0601225].

[9] T. Hambye, K. Kannike, E. Ma and M. Raidal, Phys. Rev. D **75**, 095003 (2007) [hep-ph/0609228].

[10] P. -H. Gu and U. Sarkar, Phys. Rev. D **77**, 105031 (2008) [arXiv:0712.2933 [hep-ph]].

[11] N. Sahu and U. Sarkar, Phys. Rev. D **78**, 115013 (2008) [arXiv:0804.2072 [hep-ph]].

[12] P. -H. Gu and U. Sarkar, Phys. Rev. D **78**, 073012 (2008) [arXiv:0807.0270 [hep-ph]].

[13] M. Aoki, S. Kanemura and O. Seto, Phys. Rev. Lett. **102**, 051805 (2009) [arXiv:0807.0361].

[14] J. March-Russell, C. McCabe and M. McCullough, JHEP **1003**, 108 (2010) [arXiv:0911.4489 [hep-ph]].

[15] M. Aoki, S. Kanemura, T. Shindou and K. Yagyu, JHEP **1007**, 084 (2010) [Erratum-ibid. **1011**, 049 (2010)] [arXiv:1005.5159 [hep-ph]].

[16] S. Kanemura, O. Seto and T. Shimomura, Phys. Rev. D **84**, 016004 (2011) [arXiv:1101.5713

[hep-ph]].

[17] M. Lindner, D. Schmidt and T. Schwetz, Phys. Lett. B **705**, 324 (2011) [arXiv:1105.4626 [hep-ph]].

[18] S. Kanemura, T. Nabeshima and H. Sugiyama, Phys. Lett. B **703**, 66 (2011) [arXiv:1106.2480 [hep-ph]].

[19] M. Aoki, J. Kubo, T. Okawa and H. Takano, Phys. Lett. B **707**, 107 (2012) [arXiv:1110.5403 [hep-ph]].

[20] S. Kanemura, T. Nabeshima and H. Sugiyama, Phys. Rev. D **85**, 033004 (2012) [arXiv:1111.0599 [hep-ph]].

[21] D. Schmidt, T. Schwetz and T. Toma, Phys. Rev. D **85**, 073009 (2012) [arXiv:1201.0906 [hep-ph]].

[22] S. Kanemura and H. Sugiyama, Phys. Rev. D **86**, 073006 (2012) [arXiv:1202.5231 [hep-ph]].

[23] Y. Farzan and E. Ma, Phys. Rev. D **86**, 033007 (2012) [arXiv:1204.4890 [hep-ph]].

[24] K. Kumericki, I. Picek and B. Radovcic, JHEP **1207**, 039 (2012) [arXiv:1204.6597 [hep-ph]].

[25] K. Kumericki, I. Picek and B. Radovcic, Phys. Rev. D **86**, 013006 (2012) [arXiv:1204.6599 [hep-ph]].

[26] E. Ma, Phys. Lett. B **717**, 235 (2012) [arXiv:1206.1812 [hep-ph]].

[27] G. Gil, P. Chankowski and M. Krawczyk, Phys. Lett. B **717**, 396 (2012) [arXiv:1207.0084 [hep-ph]].

[28] H. Okada and T. Toma, Phys. Rev. D **86**, 033011 (2012) arXiv:1207.0864 [hep-ph].

[29] D. Hehn and A. Ibarra, Phys. Lett. B **718**, 988 (2013) [arXiv:1208.3162 [hep-ph]].

[30] S. Baek, P. Ko, H. Okada and E. Senaha, JHEP **1409**, 153 (2014) [arXiv:1209.1685 [hep-ph]].

[31] P. S. B. Dev and A. Pilaftsis, Phys. Rev. D **86**, 113001 (2012) [arXiv:1209.4051 [hep-ph]].

[32] Y. Kajiyama, H. Okada and T. Toma, Eur. Phys. J. C **73**, 2381 (2013) [arXiv:1210.2305 [hep-ph]].

[33] M. Kohda, H. Sugiyama and K. Tsumura, Phys. Lett. B **718**, 1436 (2013) [arXiv:1210.5622 [hep-ph]].

[34] H. Okada, arXiv:1212.0492 [hep-ph].

[35] M. Gustafsson, J. M. No and M. A. Rivera, Phys. Rev. Lett. **110**, 211802 (2013) arXiv:1212.4806 [hep-ph].

[36] M. Aoki, J. Kubo and H. Takano, Phys. Rev. D **87**, no. 11, 116001 (2013) [arXiv:1302.3936

[hep-ph]].

[37] Y. Kajiyama, H. Okada and K. Yagyu, Nucl. Phys. B **874**, 198 (2013) [arXiv:1303.3463 [hep-ph]].

[38] Y. Kajiyama, H. Okada and T. Toma, Phys. Rev. D **88**, 015029 (2013) [arXiv:1303.7356].

[39] S. Kanemura, T. Matsui and H. Sugiyama, Phys. Lett. B **727**, 151 (2013) [arXiv:1305.4521 [hep-ph]].

[40] B. Dasgupta, E. Ma and K. Tsumura, Phys. Rev. D **89**, 041702 (2014) [arXiv:1308.4138 [hep-ph]].

[41] S. Baek, H. Okada and T. Toma, JCAP **1406**, 027 (2014) [arXiv:1312.3761 [hep-ph]].

[42] H. Okada, arXiv:1404.0280 [hep-ph].

[43] A. Ahriche, C. S. Chen, K. L. McDonald and S. Nasri, Phys. Rev. D **90**, no. 1, 015024 (2014) [arXiv:1404.2696 [hep-ph]].

[44] A. Ahriche, K. L. McDonald and S. Nasri, JHEP **1410**, 167 (2014) [arXiv:1404.5917 [hep-ph]].

[45] C. -S. Chen, K. L. McDonald and S. Nasri, Phys. Lett. B **734**, 388 (2014) [arXiv:1404.6033 [hep-ph]].

[46] S. Kanemura, T. Matsui and H. Sugiyama, Phys. Rev. D **90**, 013001 (2014) [arXiv:1405.1935 [hep-ph]].

[47] H. Okada and Y. Orikasa, Phys. Rev. D **90**, no. 7, 075023 (2014) [arXiv:1407.2543 [hep-ph]].

[48] S. Fraser, E. Ma and O. Popov, Phys. Lett. B **737**, 280 (2014) [arXiv:1408.4785 [hep-ph]].

[49] H. Okada, T. Toma and K. Yagyu, Phys. Rev. D **90**, no. 9, 095005 (2014) [arXiv:1408.0961 [hep-ph]].

[50] S. Baek, H. Okada and K. Yagyu, JHEP **1504**, 049 (2015) [arXiv:1501.01530 [hep-ph]].

[51] L. G. Jin, R. Tang and F. Zhang, Phys. Lett. B **741**, 163 (2015) [arXiv:1501.02020 [hep-ph]].

[52] P. Culjak, K. Kumericki and I. Picek, Phys. Lett. B **744**, 237 (2015) [arXiv:1502.07887 [hep-ph]].

[53] H. Okada, arXiv:1503.04557 [hep-ph].

[54] C. Q. Geng and L. H. Tsai, arXiv:1503.06987 [hep-ph].

[55] H. Okada, N. Okada and Y. Orikasa, arXiv:1504.01204 [hep-ph].

[56] C. Q. Geng, D. Huang and L. H. Tsai, Phys. Lett. B **745**, 56 (2015) [arXiv:1504.05468 [hep-ph]].

[57] A. Ahriche, K. L. McDonald, S. Nasri and T. Toma, Phys. Lett. B **746**, 430 (2015) [arXiv:1504.05755 [hep-ph]].

[58] D. Restrepo, A. Rivera, M. Sánchez-Peláez, O. Zapata and W. Tangarife, arXiv:1504.07892 [hep-ph].

[59] S. Kashiwase, H. Okada, Y. Orikasa and T. Toma, arXiv:1505.04665 [hep-ph].

[60] Y. H. Ahn and H. Okada, Phys. Rev. D **85**, 073010 (2012) [arXiv:1201.4436 [hep-ph]].

[61] E. Ma, A. Natale and A. Rashed, Int. J. Mod. Phys. A **27**, 1250134 (2012) [arXiv:1206.1570 [hep-ph]].

[62] Y. Kajiyama, H. Okada and K. Yagyu, JHEP **10**, 196 (2013) arXiv:1307.0480 [hep-ph].

[63] A. E. Carcamo Hernandez, I. d. M. Varzielas, S. G. Kovalenko, H. Päs and I. Schmidt, Phys. Rev. D **88**, 076014 (2013) [arXiv:1307.6499 [hep-ph]].

[64] E. Ma and A. Natale, Phys. Lett. B **723**, 403 (2014) [arXiv:1403.6772 [hep-ph]].

[65] M. Aoki and T. Toma, JCAP **1409**, 016 (2014) [arXiv:1405.5870 [hep-ph]].

[66] E. Ma, Phys. Lett. B **741**, 202 (2015) [arXiv:1411.6679 [hep-ph]].

[67] E. Ma, arXiv:1504.02086 [hep-ph].

[68] A. E. Carcamo Hernandez, RMartinez and F. Ochoa, arXiv:1309.6567 [hep-ph].

[69] E. Ma, Phys. Rev. Lett. **112**, 091801 (2014) [arXiv:1311.3213 [hep-ph]].

[70] H. Okada and K. Yagyu, Phys. Rev. D **89**, 053008 (2014) [arXiv:1311.4360 [hep-ph]].

[71] S. Baek, H. Okada and T. Toma, Phys. Lett. B **732**, 85 (2014) [arXiv:1401.6921 [hep-ph]].

[72] H. Okada and K. Yagyu, Phys. Rev. D **90**, no. 3, 035019 (2014) [arXiv:1405.2368 [hep-ph]].

[73] F. Bonnet, M. Hirsch, T. Ota and W. Winter, JHEP **1207**, 153 (2012) [arXiv:1204.5862 [hep-ph]].

[74] D. Aristizabal Sierra, A. Degee, L. Dorame and M. Hirsch, JHEP **1503**, 040 (2015) [arXiv:1411.7038 [hep-ph]].

[75] H. Davoudiasl and I. M. Lewis, Phys. Rev. D **90**, no. 3, 033003 (2014) [arXiv:1404.6260 [hep-ph]].

[76] M. Lindner, S. Schmidt and J. Smirnov, arXiv:1405.6204 [hep-ph].

[77] H. Okada and Y. Orikasa, arXiv:1412.3616 [hep-ph].

[78] K. S. Babu and C. Macesanu, Phys. Rev. D **67**, 073010 (2003) [hep-ph/0212058].

[79] D. Aristizabal Sierra and D. Restrepo, JHEP **0608**, 036 (2006) [hep-ph/0604012].

[80] D. Aristizabal Sierra and M. Hirsch, JHEP **0612**, 052 (2006) [hep-ph/0609307].

[81] M. Nebot, J. F. Oliver, D. Palao and A. Santamaria, Phys. Rev. D **77**, 093013 (2008) [arXiv:0711.0483 [hep-ph]].

[82] R. Bouchand and A. Merle, JHEP **1207**, 084 (2012) [arXiv:1205.0008 [hep-ph]].

[83] Y. Kajiyama, H. Okada and K. Yagyu, Nucl. Phys. B **887**, 358 (2014) [arXiv:1309.6234 [hep-ph]].

[84] K. L. McDonald, JHEP **1311**, 131 (2013) [arXiv:1310.0609 [hep-ph]].

[85] E. Ma, Phys. Lett. B **732**, 167 (2014) [arXiv:1401.3284 [hep-ph]].

[86] D. Schmidt, T. Schwetz and H. Zhang, Nucl. Phys. B **885**, 524 (2014) [arXiv:1402.2251 [hep-ph]].

[87] J. Herrero-Garcia, M. Nebot, N. Rius and A. Santamaria, Nucl. Phys. B **885**, 542 (2014) [arXiv:1402.4491 [hep-ph]].

[88] A. Ahriche, S. Nasri and R. Soualah, Phys. Rev. D **89**, 095010 (2014) [arXiv:1403.5694 [hep-ph]].

[89] H. N. Long and V. V. Vien, Int. J. Mod. Phys. A **29**, no. 13, 1450072 (2014) [arXiv:1405.1622 [hep-ph]].

[90] V. Van Vien, H. N. Long and P. N. Thu, arXiv:1407.8286 [hep-ph].

[91] S. Weinberg, Phys. Rev. Lett. **110**, no. 24, 241301 (2013) [arXiv:1305.1971 [astro-ph.CO]].

[92] Y. Chikashige, R. N. Mohapatra and R. D. Peccei, Phys. Lett. B **98**, 265 (1981); A. Adulpravitchai, P. H. Gu and M. Lindner, Phys. Rev. D **82**, 073013 (2010).

[93] D. Cadamuro and J. Redondo, JCAP **1202**, 032 (2012) [arXiv:1110.2895 [hep-ph]].

[94] A. Pilaftsis, Phys. Rev. D **49**, 2398 (1994) [hep-ph/9308258].

[95] K. Cheung, W. Y. Keung and T. C. Yuan, Phys. Rev. D **89**, no. 1, 015007 (2014) [arXiv:1308.4235 [hep-ph]].

[96] R. Battye and A. Moss, Phys. Rev. D **82**, 023521 (2010) [arXiv:1005.0479 [astro-ph.CO]].

[97] Z. Maki, M. Nakagawa and S. Sakata, Prog. Theor. Phys. **28**, 870 (1962).

[98] B. Pontecorvo, Sov. Phys. JETP **26**, 984 (1968) [Zh. Eksp. Teor. Fiz. **53**, 1717 (1967)].

[99] M. C. Gonzalez-Garcia, M. Maltoni and T. Schwetz, JHEP **1411**, 052 (2014) [arXiv:1409.5439 [hep-ph]].

[100] E. Arganda and M. J. Herrero, Phys. Rev. D **73**, 055003 (2006) [hep-ph/0510405].

[101] T. Toma and A. Vicente, JHEP **1401**, 160 (2014) [arXiv:1312.2840 [hep-ph]].

[102] T. A. Chowdhury and S. Nasri, arXiv:1506.00261 [hep-ph].

[103] G. Aad *et al.* [ATLAS Collaboration], JHEP **1503**, 041 (2015) [arXiv:1412.0237 [hep-ex]].

[104] P. P. Giardino, K. Kannike, M. Raidal and A. Strumia, Phys. Lett. B **718**, 469 (2012) [arXiv:1207.1347 [hep-ph]].

[105] D. Carmi, A. Falkowski, E. Kuflik, T. Volansky and J. Zupan, JHEP **1210**, 196 (2012) [arXiv:1207.1718 [hep-ph]].

[106] J. Ellis and T. You, JHEP **1209**, 123 (2012) [arXiv:1207.1693 [hep-ph]].

[107] G. Aad *et al.* [ATLAS Collaboration], Phys. Rev. D **90**, no. 11, 112015 (2014) [arXiv:1408.7084 [hep-ex]].

[108] G. Aad *et al.* [ATLAS Collaboration], Phys. Rev. D **91**, no. 1, 012006 (2015) [arXiv:1408.5191 [hep-ex]].

[109] G. Aad *et al.* [ATLAS Collaboration], arXiv:1412.2641 [hep-ex].

[110] G. Aad *et al.* [ATLAS Collaboration], JHEP **1501**, 069 (2015) [arXiv:1409.6212 [hep-ex]].

[111] The ATLAS collaboration, ATLAS-CONF-2014-061, ATLAS-COM-CONF-2014-080.

[112] V. Khachatryan *et al.* [CMS Collaboration], Eur. Phys. J. C **75**, no. 5, 212 (2015) [arXiv:1412.8662 [hep-ex]].

[113] S. Heinemeyer *et al.* [LHC Higgs Cross Section Working Group Collaboration], arXiv:1307.1347 [hep-ph].

[114] J. R. Ellis, M. K. Gaillard and D. V. Nanopoulos, Nucl. Phys. B **106**, 292 (1976).

[115] M. A. Shifman, A. I. Vainshtein, M. B. Voloshin and V. I. Zakharov, Sov. J. Nucl. Phys. **30**, 711 (1979) [Yad. Fiz. **30**, 1368 (1979)].

[116] A. Djouadi, Phys. Rept. **457**, 1 (2008) [hep-ph/0503172].

[117] M. Carena, I. Low and C. E. M. Wagner, JHEP **1208**, 060 (2012) [arXiv:1206.1082 [hep-ph]].

[118] C. S. Chen, C. Q. Geng, D. Huang and L. H. Tsai, Phys. Rev. D **87**, 075019 (2013) [arXiv:1301.4694 [hep-ph]].

[119] K. Griest and D. Seckel, Phys. Rev. D **43**, 3191 (1991).

[120] P. A. R. Ade *et al.* [Planck Collaboration], Astron. Astrophys. (2014) [arXiv:1303.5076 [astro-ph.CO]].

[121] P. Gondolo and G. Gelmini, Nucl. Phys. B **360**, 145 (1991).

[122] J. Edsjo and P. Gondolo, Phys. Rev. D **56**, 1879 (1997) [hep-ph/9704361].

[123] J. Hisano, K. Ishiwata and N. Nagata, Phys. Rev. D **82**, 115007 (2010) [arXiv:1007.2601 [hep-ph]].

[124] T. Abe and R. Sato, JHEP **1503**, 109 (2015) [arXiv:1501.04161 [hep-ph]].

[125] G. Belanger, F. Boudjema, A. Pukhov and A. Semenov, Comput. Phys. Commun. **185**, 960 (2014) [arXiv:1305.0237 [hep-ph]].

[126] D. S. Akerib *et al.* [LUX Collaboration], Phys. Rev. Lett. **112**, 091303 (2014) [arXiv:1310.8214 [astro-ph.CO]].

[127] S. Baek, P. Ko and W. I. Park, JHEP **1202**, 047 (2012) [arXiv:1112.1847 [hep-ph]].

[128] S. Baek, P. Ko, W. I. Park and E. Senaha, JHEP **1305**, 036 (2013) [arXiv:1212.2131 [hep-ph]].

[129] J. M. Cline and K. Kainulainen, JCAP **1301**, 012 (2013) [arXiv:1210.4196 [hep-ph]].

[130] J. M. Cline, K. Kainulainen, P. Scott and C. Weniger, Phys. Rev. D **88**, 055025 (2013) [arXiv:1306.4710 [hep-ph]].

[131] K. Cheung and O. Seto, Phys. Rev. D **69**, 113009 (2004) [hep-ph/0403003].

[132] The ATLAS collaboration [ATLAS Collaboration], ATLAS-CONF-2015-004, ATLAS-COM-CONF-2015-004.